

1 **GF11 cooperates with IKAROS/IKZF1 to activate gene expression in T-cell acute lymphoblastic**  
2 **leukemia**

3

4 **Wenxiang Sun<sup>1,2</sup>, Jingtao Guo<sup>2,3,§</sup>, David McClellan<sup>2,3</sup>, Alexandra Poeschla<sup>1</sup>, Diana Bareyan<sup>2</sup>, Mattie**  
5 **J. Casey<sup>2,3</sup>, Bradley R. Cairns<sup>2,3,4</sup>, Dean Tantin<sup>1,2,\*</sup> and Michael E. Engel<sup>2,3,5,6,Ψ,\*</sup>**

6

7 <sup>1</sup>Department of Pathology, University of Utah School of Medicine, Salt Lake City, UT 84112, USA.

8 <sup>2</sup>Huntsman Cancer Institute, University of Utah School of Medicine, Salt Lake City, UT 84112, USA.

9 <sup>3</sup>Department of Oncological Sciences, University of Utah School of Medicine, Salt Lake City, UT 84112,  
10 USA.

11 <sup>4</sup>Howard Hughes Medical Institute, University of Utah School of Medicine, Salt Lake City, Utah.

12 <sup>5</sup>Department of Pediatrics, University of Utah School of Medicine, Salt Lake City, UT 84112, USA.

13 <sup>6</sup>Primary Children's Hospital, Salt Lake City, UT 84112, USA.

14

15 \*To whom the correspondence should be addressed. [Tel:+1](tel:+14349245292) (434)924-5292 or (434)924-5105. Email:

16 [mee2mj@hscmail.mcc.virginia.edu](mailto:mee2mj@hscmail.mcc.virginia.edu) . Correspondence may also be addressed to Dean Tantin [Tel:+1](tel:+18015873035)

17 (801)587-3035. Email: [dean.tantin@path.utah.edu](mailto:dean.tantin@path.utah.edu) .

18

19 **KEYWORDS:** GF11; IKAROS; NOTCH3; T-cell Acute Lymphoblastic Leukemia (T-ALL)

20

21 <sup>Ψ</sup> Present address: Michael E. Engel, Department of Pediatrics, Division of Pediatric Hematology/Oncology,

22 P.O. Box 800386, University of Virginia School of Medicine, Charlottesville, VA 22908-0386, USA.

23 <sup>§</sup> Present address: Jingtao Guo, Department of Surgery, Division of Urology, University of Utah School of

24 Medicine, Salt Lake City, UT 84112, USA.

25 **Abstract (168 words)**

26 Growth factor independence-1 (GFI1) is a transcriptional repressor and master regulator of normal and  
27 malignant hematopoiesis. Repression by GFI1 is attributable to recruitment of LSD1-containing protein  
28 complexes via its SNAG domain. However, the full complement of GFI1 partners in transcriptional control  
29 is not known. We show that in T-ALL cells, GFI1 and IKAROS are transcriptional partners that co-occupy  
30 regulatory regions of hallmark T cell development genes. Transcriptional profiling reveals a subset of genes  
31 directly transactivated through the GFI1—IKAROS partnership. Among these is *NOTCH3*, a key factor in  
32 T-ALL pathogenesis. Surprisingly, *NOTCH3* transactivation by GFI1 and IKAROS requires the GFI1  
33 SNAG domain but occurs independent of SNAG—LSD1 binding. GFI1 variants deficient in LSD1 binding  
34 fail to transactivate *NOTCH3*, but conversely, small molecules that disrupt the SNAG—LSD1 interaction  
35 while leaving the SNAG primary structure intact stimulate *NOTCH3* expression. These results identify a  
36 non-canonical transcriptional control mechanism in T-ALL which supports GFI1-mediated transactivation  
37 in partnership with IKAROS and suggest competition between LSD1-containing repressive complexes and  
38 others favoring transactivation.

## 39 Introduction

40 Growth factor independence-1 (GFI1) is a zinc finger transcription factor which plays essential roles in  
41 normal and malignant myeloid and lymphoid hematopoiesis (Hock, Hamblen et al., 2004, Zeng, Yucel et  
42 al., 2004). Germline *GFI1* mutations cause severe congenital neutropenia (Person, Li et al., 2003), while  
43 *Gfi1* null mice show impaired T cell and neutrophil differentiation (Hock, Hamblen et al., 2003, Karsunky,  
44 Zeng et al., 2002, Yucel, Karsunky et al., 2003). In acute myelogenous leukemia (AML), *GFI1* mRNA  
45 expression can be used to stratify patient survival, while *GFI1* displays a dose-dependent impact on the  
46 pace of leukemic progression brought on by onco-fusion proteins, MLL-AF9 and NUP98-HOXD13 (Hones,  
47 Botezatu et al., 2016, Volpe, Walton et al., 2017). Notably, a GFI1 variant, GFI136N, generated from a  
48 single nucleotide polymorphism expressed in 3-7% of the Caucasian population, is disproportionately  
49 observed in AML patients and increases risk for AML development by 60% relative to the more common  
50 GFI136S variant (Khandanpour, Krongold et al., 2012). *GFI1* mRNA is also elevated in samples from  
51 patients with early T cell precursor acute lymphoblastic leukemia (ETP-ALL) who display a positive  
52 NOTCH signature (Khandanpour, Phelan et al., 2013). ETP-ALL is a high-risk subgroup of T-ALL  
53 (Coustan-Smith, Mullighan et al., 2009, Zhang, Ding et al., 2012), which itself is an aggressive form of  
54 acute leukemia characterized by the expansion of immature lymphoid precursor cells (Terwilliger & Abdul-  
55 Hay, 2017). The precise role of GFI1 in T-ALL is not clear.

56

57 T-ALL has a high incidence of relapse, and survival following disease recurrence is dismal. Abberant  
58 activation of NOTCH signaling is a unifying theme in T-ALL, and arises either from mutations in NOTCH  
59 receptors or NOTCH regulators. Normally, in response to ligand binding, NOTCH receptors are cleaved  
60 by  $\gamma$ -secretase to liberate their intracellular domains (NICD). NICD then partners with nuclear factors to  
61 direct the expression of NOTCH target genes. *NOTCH1*-activating mutations are found in approximately  
62 60% of T-ALL cases (Ferrando, 2010). While  $\gamma$ -secretase inhibitors (GSIs) have shown anti-leukemic  
63 activity *in vitro* and in murine models, they have not been integrated into T-ALL treatment protocols  
64 because of dose limiting gastrointestinal toxicity and poor anti-leukemic efficacy (Golde, Koo et al., 2013).

65 Like NOTCH1, NOTCH3 promotes T cell lineage specification and leukemogenesis. *NOTCH3*-activating  
66 mutations have been identified in approximately 5% of T-ALL cases and NOTCH3 blocking antibodies  
67 exhibit potent anti-leukemic effect in T-ALL (Bellavia, Campese et al., 2000, Bellavia, Campese et al.,  
68 2002, Bernasconi-Elias, Hu et al., 2016, Waegemans, Van de Walle et al., 2014, Xu, Choi et al., 2015).  
69 Moreover, abnormal expression and/or activation of *NOTCH3* is seen in T-ALL patient samples lacking  
70 *NOTCH1*-activating mutations, reinforcing NOTCH signaling as critical for T-ALL pathogenesis and  
71 suggesting *NOTCH3* and factors controlling its expression could represent alternative therapeutic targets in  
72 this disease (Choi, Severson et al., 2017, Tottone, Zhdanovskaya et al., 2019). The development of new  
73 therapeutic strategies for T-ALL depends upon deeper understanding of its molecular underpinnings.

74

75 Here, we identify IKAROS as a frequent DNA binding partner for GFI1. GFI1 and IKAROS do not interact  
76 in classical co-immunoprecipitation (co-IP) assays, but their proximity relationship is impaired by the  
77 N383S mutation that impairs GFI1 DNA binding and the N159A mutation that impairs IKAROS DNA  
78 binding. In contrast, their interaction is not affected by LSD1 binding-deficient GFI1 variants including  
79 GFI1-P2A, -K8L or -ΔSNAG. We identify a strong, genome-wide correlation between GFI1- and  
80 IKAROS-regulated genes through ChIP-Seq. Genes co-occupied by GFI1 and IKAROS encode hallmark  
81 T cell development proteins such as NOTCH3, CD3, GFI1 itself, c-MYC, C-MYB and HES1. Gene  
82 expression profiling by RNA-Seq identifies a cluster of genes activated by ectopic GFI1 expression and  
83 repressed with IKAROS knockout. Interestingly, these genes include the direct GFI1/IKAROS target  
84 *NOTCH3*, a critical oncogenic factor in T-ALL. Using both CCRF-CEM and SUP-T1 T-ALL cells, we  
85 show that inducible expression of either GFI1 or IKAROS elevates NOTCH3 cell surface expression, while  
86 acute degradation of IKAROS through an IKAROS inhibitor or CRISPR/Cas9-mediated IKAROS  
87 knockout significantly attenuates GFI1-mediated NOTCH3 induction. Increased NOTCH3 cell surface  
88 expression depends upon SNAG domain amino acids that enable interaction with LSD1. Yet, LSD1  
89 inhibition and disruption of the SNAG—LSD1 interaction augments *NOTCH3* expression, suggesting that  
90 LSD1 competes with activators of NOTCH3 expression mediated by the GFI SNAG domain. Together,

91 these results identify a noncanonical transactivation mechanism for GFI1, working in partnership with  
92 IKAROS to promote expression of *NOTCH3* and related T cell development genes, and providing new  
93 insights for therapeutic targeting in T-ALL.

## 94 **Results**

### 95 **GFI1 proximitome proteomics in T-ALL cells**

96 To identify potential GFI1 cooperating proteins in T-ALL, we applied the BioID (Biotin Identification)  
97 proximity-dependent labeling method to screen for vicinal proteins (Figure 1A). We generated doxycycline-  
98 inducible, GFI1-BirA\*-expressing CCRF-CEM cells. In parallel, cells transduced with empty vector or  
99 BirA\* only were generated as controls (Figure 1B). Cells were incubated in biotin-containing medium,  
100 treated with doxycycline and lysates prepared. Biotinylated proteins were collected with streptavidin  
101 Sepharose beads and surveyed for known GFI1 interacting partners. As expected, we detected comparable  
102 biotinylation of GFI1-BirA\* and BirA\*, suggesting the presence of GFI1 protein structure does not interfere  
103 with the formation of reactive biotin-AMP by BirA\* in the fusion protein. Moreover, we find an altered  
104 pattern of biotinylated proteins when BirA\* activity is tethered to GFI1, and enrichment for known GFI1  
105 interacting partners, LSD1 and CoREST among biotinylated proteins in cells expressing GFI1-BirA\* vs.  
106 BirA\* control (Figure 1C). These data validate the technique for detecting GFI1 proximity partners  
107 proteome-wide.

108 To identify the complete cohort of GFI1 proximity partners, biotinylated proteins were purified on  
109 streptavidin (SAv)-Sepharose beads and subjected to unbiased, proteome-wide LC-MS/MS (Figure 1A).  
110 Three replicates were performed for each condition (Vector, BirA\* and GFI1-BirA\*). A total of 502  
111 interacting proteins were identified that demonstrated both increased mass spectrometry intensity in the  
112 presence of doxycycline compared to empty vector control and a BirA\* vs GFI1- BirA\* *P*-value of <0.05  
113 (Supplemental Table S1). Proximity partners were analyzed as previously described (McClellan, Casey et  
114 al., 2019). A volcano plot showing fold change in average sum read intensities ( $\log_2$  (GFI1-WT/BirA\*))  
115 relative to *P*-value ( $-\log_{10}$  *P*-value) is shown in Figure 2A. Being covalently tethered to BirA\*, the  
116 placement of GFI1 in the top right corner of the plot is an important quality control, signifying the most  
117 statistically significant *P*-value and most abundantly enriched protein in the data set. Among biotinylated  
118 proteins, known GFI1 partners LSD1 (KDM1A), CoREST (RCOR1), STAG1, BCL11A and HMG20B  
119 were enriched when comparing GFI1-BirA\* to BirA\* only (Figure 2A, shown in red). Among newly-

120 identified GFI1 proximity partners, the strongest overall by fold-enrichment was for IKZF1/IKAROS  
121 (Figure 2A). To identify possible functional protein associations, we clustered the top 40 GFI1-proximate  
122 proteins using the STRING functional protein—protein association network (Szklarczyk, Gable et al.,  
123 2019). The majority of these proteins were annotated as being nuclear and involved in regulating gene  
124 expression (Figure 2B, red and blue circles respectively). Notably, STRING output linked GFI1 directly to  
125 LSD1 and CoREST, as expected (Figure 2B), but placed IKAROS more remotely, arguing against a direct  
126 interaction with GFI1 (Figure 2B).

127

### 128 **The GFI1—IKAROS interaction requires intact GFI1 and IKAROS DNA binding**

129 We validated the proximity relationship between IKAROS and GFI1 through Western blotting. First, we  
130 tested if N-terminal GFI1 mutations known to block binding to LSD1 also block the ability to transfer biotin  
131 moieties to IKAROS. GFI1 mutations that block LSD1 binding did not affect IKAROS proximity labeling  
132 (Figure 3A). Additionally, GFI1 and IKAROS failed to interact using a variety of traditional co-  
133 immunoprecipitation conditions (Figure 3B and data not shown). One possible explanation for the  
134 discrepancy could be that GFI1 and IKAROS co-occupy nearby DNA binding sites at common target genes  
135 such that their proximity enables biotin moieties to be frequently transferred from GFI1-BirA\* to IKAROS  
136 even though the two proteins do not interact directly in solution. Similarly, GFI1 and IKAROS could  
137 occupy sites distant from one another but brought together through interactions involving a shared protein  
138 complex. Both models predict that the proximity relationship between GFI1 and IKAROS would require  
139 both proteins to bind DNA and that a defect in DNA binding by either protein would attenuate the proximity  
140 relationship between them. Previous work on GFI1 and IKAROS has identified specific domains and  
141 mutants that control DNA binding activity (Kuehn, Boisson et al., 2016, Zarebski, Velu et al., 2008). We  
142 established these DNA-binding deficient mutations in GFI1 (N383S in rat GFI1, which corresponds to  
143 N382S in human GFI1) and IKAROS (N159A) and used them to interrogate the GFI1—IKAROS proximity  
144 relationship. GFI1-N383S-BirA\* reduced proximity labeling of wild type IKAROS (Figure 3C). Likewise,  
145 we observed a comparable reduction in proximity labeling of IKAROS-N159A when when tested with wild

146 type GFI1-BirA\*. When both DNA-binding deficient mutants were combined, the proximity relationship  
147 between GFI1 and IKAROS is abolished (Figure 3C). These results indicate that the proximity relationship  
148 between GFI1 and IKAROS relies upon their shared ability to bind DNA and suggests a mechanism for  
149 GFI1 and IKAROS to cooperate to control a common set of genes through near or distant regulatory regions.

150

### 151 **GFI1 and IKAROS associate with common genes, including genes associated with T cell development**

152 To further study the interplay between GFI1 and IKAROS, we conducted ChIP-Seq using CCRF-CEM  
153 cells expressing 3×FLAG-tagged GFI1 or IKAROS (GFI1-3×FLAG or IKAROS-3×FLAG) under  
154 doxycycline-inducible control. FLAG immunoblotting confirmed inducible and comparable expression of  
155 the two proteins (Figure 4A). Two replicates each for GFI1 and IKAROS ChIP were performed. Sequencing  
156 of the ChIP material resulted in 25,674 total GFI1 and 52,759 IKAROS peaks. The signals from input, GFI1  
157 ChIP-Seq and IKAROS ChIP-Seq replicates were highly correlated, with Spearman correlation R-  
158 values >0.8. Further, the GFI1 and IKAROS ChIP-Seq signals were also highly correlated, with R  
159 values >0.75. (Supplementary Figure S1A). Principal component analysis of the bound peaks also indicated  
160 that the inputs and ChIP replicates from the two cells lines were more similar to each other compared to the  
161 other samples (Supplementary Figure S1B). Approximately 80% of GFI1-bound peaks overlap (at least one  
162 bp) with peaks bound by IKAROS (Figure 4B), suggesting that they regulate common targets. To  
163 investigate this more closely, we centered binding peaks from either or both ChIP experiments (57,841  
164 peaks) by peak summit, and arranged them as a heatmap from strongest to weakest GFI1 binding (Figure  
165 4C, left side) and IKAROS binding (Figure 4C, right side), indicating an overall correlation between the  
166 strength of GFI1 and IKAROS binding. Motif analysis using all identified peaks showed that GFI1 and  
167 IKAROS shared four of the top five most significant binding motifs (Supplementary Figure S1C), again  
168 suggesting common gene binding. Among the top shared motifs is FLI1, an Ets transcription factor  
169 (consensus TTCC or GGAA reverse complement). Out of the top 20 enriched motifs for the two datasets,  
170 14 and 15 Ets transcription motifs were present (Supplementary Figure S1C and data not shown). IKAROS  
171 is known to interact with Ets motifs (Zhang, Jackson et al., 2011).



172 GFI1 and IKAROS play crucial roles in hematopoiesis, including in T cells (Georgopoulos, Bigby  
173 et al., 1994, Shi, Kalupahana et al., 2013, Tinsley, Hong et al., 2013). Consistently, gene ontology (GO)  
174 analysis of genes within 6 kb of the GFI1- and IKAROS-bound peaks (using GREAT v4.0.4) identifies  
175 hematopoiesis and TCR recombination as common terms (Supplemental Table S2). Example bound targets  
176 are shown in Figure 4D, including genes encoding key transcription factors required for T cell development  
177 such as *GFI1* itself, *MYC*, *MYB*, *HES1*, *RUNX3* and *TCF3*. Other examples include *NOTCH3* and genes in  
178 the *CD3* cluster. Figure 4D also shows previously published RNA-Seq data (Quentmeier, Pommerenke et  
179 al., 2019) indicating that these genes are all expressed in CCRF-CEM cells.

180

### 181 **GFI1 and IKAROS positively regulate a subset of target genes**

182 We used bulk RNA-Seq with GFI1-3×FLAG CCRF-CEM cells to identify changes in gene expression  
183 associated with either ectopic GFI1 expression or CRISPR-mediated IKAROS knockout. For knockout, we  
184 transfected GFI1-3×FLAG cells with CRISPR RNPs containing Cas9 protein, fluorescently-conjugated  
185 tracrRNA and either a nonspecific or *IKAROS*-specific sgRNA. Successfully transfected cells were sorted  
186 on the following day and cultured for an additional 9 days before treatment with doxycycline or vehicle for  
187 24 hrs (see methods). This resulted in robust knockout using specific but not control RNPs (Figure 5A). A  
188 similar knockout strategy targeting GFI1 resulted in lethality in CCRF-CEM cells (not shown),  
189 underscoring its critical pro-survival role, and for this reason was not pursued further. Three independent  
190 replicates were performed for each of the four conditions, with the exception of vehicle-treated IKAROS  
191 knockout with two replicates. Between 21.7 and 28.2 million RNA-Seq reads were generated for each  
192 condition, wherein 88.6 to 90.3% of these aligned uniquely to the human *Hg38* reference genome.  
193 Approximately 99% of the reads within coding regions aligned to the correct strand (Supplemental Table  
194 S3). Hierarchical clustering of the top 500 most significantly differentially regulated genes across all the  
195 conditions (ranked based on *P*-value) revealed groups of genes repressed and activated by the different  
196 conditions. For example, a large number of genes are de-repressed with IKAROS knockout and/or repressed

197 with GFI1 overexpression (Figure 5B, clusters 1, 2 ,3). Another group, not strongly affected by GFI1, was  
198 repressed with IKAROS knockout (cluster 5). However, a small group of 38 genes (cluster 4) were induced  
199 by GFI1 overexpression (Figure 5B). This same group of genes was also repressed with IKAROS knockout.  
200 Interestingly, when ectopic GFI1 expression and IKAROS knockout were combined, the induction of these  
201 genes was significantly blunted, suggesting IKAROS is required for GFI1-mediated transactivation (Figure  
202 5B). These genes include *RAG1* and *NOTCH3* (Supplemental Table S4). Intersecting this set of positively  
203 regulated genes with the ChIP-Seq data reveals that 68.4% (26 of 38 total genes in cluster 4) have peaks  
204 for GFI1 and IKAROS located <10 kb from their transcription start sites, strongly suggesting they are direct  
205 targets of both GFI1 and IKAROS (Supplemental Table S4). 34.2% of these genes (13/38) show promoter  
206 binding (<500 bp from TSS) of both proteins. RNA-Seq genome tracks for *NOTCH3* are shown in Figure  
207 5C alongside the GFI1 and IKAROS ChIP-Seq reads. Strong and overlapping GFI1 and IKAROS peaks  
208 are present in the 5' region of the gene. In the RNA-seq, *NOTCH3* is induced by ectopic GFI1 expression  
209 and inhibited by IKAROS knockout, while the combination significantly blunts induction by GFI1. No such  
210 changes were observed for *NOTCH1* or *NOTCH2*, which show some GFI1 and IKAROS association but  
211 constitutive expression, or for *NOTCH4*, which shows no binding and is not expressed in CCRF-CEM cells  
212 (Supplementary Figure 2).

213

### 214 **GFI1 and IKAROS cooperatively regulate NOTCH3**

215 A model in which GFI1 and IKAROS interact on DNA to induce the expression of specific genes predicts  
216 that overexpression of either protein should induce target gene expression. Both GFI1 and IKAROS interact  
217 with the *NOTCH3* gene. In addition, *NOTCH3* activating mutations can trigger T-ALL development  
218 (Bernasconi-Elias et al., 2016, Choi et al., 2017, Tottone et al., 2019). For these reasons, and because its  
219 surface expression can easily be measured using flow cytometry, we used *NOTCH3* as an example target  
220 gene. We treated CCRF-CEM cells that inducibly express GFI1-3×FLAG with doxycycline and followed  
221 surface NOTCH3 expression as a time course using flow cytometry. NOTCH3 was low but detectable in  
222 untreated cells (Figure 6A, 0h), with expression increasing during the 48 hour treatment course. Expression

223 increased both as measured by the percentage of positive cells (not shown), and as measured by mean  
224 fluorescence intensity (MFI). CCRF-CEM cells inducibly expressing IKAROS-3×FLAG were similarly  
225 able to increase cell surface expression of NOTCH3 (Figure 6B). We then replaced the GFII1 lentiviral  
226 construct with a truncation mutant in which the SNAG domain was deleted ( $\Delta$ SNAG) or with a SNAG  
227 domain point mutant that no longer interacts with LSD1 to mediate transcriptional repression (P2A)  
228 (Grimes, Chan et al., 1996, Velinder, Singer et al., 2017). Unexpectedly, these mutant forms of GFII1 no  
229 longer augment surface NOTCH3 expression (Figure 6C). These results suggest that GFII1 and IKAROS  
230 collaborate to transactivate the *NOTCH3* gene, and that GFII1 does so, at least in part, through residues that  
231 are also important to recruit LSD1. To more directly determine the role of LSD1 in GFII1-mediated  
232 NOTCH3 induction in CCRF-CEM cells, we utilized the non-competitive LSD1 inhibitor, SP-2509 (Fiskus,  
233 Sharma et al., 2017, Inui, Zhao et al., 2017). Surprisingly, NOTCH3 expression significantly increased in  
234 cells treated with SP-2509 compared to DMSO vehicle control even without doxycycline treatment (Figure  
235 6D). Doxycycline-induced GFII1 expression cooperated with SP-2509 to further increase NOTCH3  
236 expression at 24 but not 48 hr (Figure 6D). We also obtained similar results using SUP-T1, a different T-  
237 ALL cell line. Doxycycline-induced GFII1 expression or LSD1 inhibition with SP-2509 elevated surface  
238 levels of NOTCH3 (Figure 7A).

239 Notably, results obtained using SNAG domain mutants ( $\Delta$ SNAG and P2A) are the reverse of those  
240 obtained with SP-2509, where the SNAG domain remains intact. We hypothesized this positive impact of  
241 SP-2509 could represent targeted disruption of the interaction between LSD1 and the SNAG domain to  
242 enable alternative interactions involving candidate co-activators. Small molecule inhibitors of LSD1 can  
243 disrupt binding between GFII1 and LSD1 (Maiques-Diaz, Spencer et al., 2018). Further, we have previously  
244 shown the SNAG domain is sufficient for LSD1 binding and that dimethyl modification at lysine 8 (K8me2)  
245 of the SNAG domain strongly favors LSD1 binding in an *in vitro* binding assay. We deployed this assay  
246 (Figure 7B, left panel) to test the impact of SP-2509 on SNAG—LSD1 binding. We find that SP-2509  
247 completely abolishes binding between LSD1 and a biotinylated K8me2-SNAG peptide (Figure 7B, right

248 panel). These results suggest the SNAG—LSD1 interaction can be modulated to enable competition  
249 between LSD1 and one or more unknown proteins for SNAG domain binding and regulation of GFII1-  
250 mediated transcriptional output.

251 We then tested the effect of IKAROS loss on GFII1-induced NOTCH3 expression using GFII1-  
252 3×FLAG CCRF-CEM cells. Lenalidomide is well-documented to rapidly and efficiently trigger  
253 degradation of IKAROS (Lu, Middleton et al., 2014). Induction of cell surface NOTCH3 expression was  
254 significantly impaired by Lenalidomide treatment compared with DMSO control (Figure 7C).  
255 Immunoblotting confirmed the rapid loss of IKAROS protein and unaltered expression of ectopic GFII1 in  
256 the presence of Lenalidomide (Supplementary Figure S3A-B). We obtained similar results using the same  
257 cells instead electroporated with IKAROS CRISPR RNPs (Figure 7D, Supp. Figure 3C-D). These results  
258 strongly suggest that IKAROS and GFII1 act in a cooperative fashion to transactivate a specific subset of  
259 genes which includes *NOTCH3*, and given the tumor promoting role of constitutively active NOTCH3  
260 could provide a new direction for therapeutic development in T-ALL (Figure 8).

## 261 Discussion

262 Identifying the molecular determinants of T cell development furthers understanding of T-ALL  
263 pathogenesis (Rothenberg & Taghon, 2005). The zinc finger transcription factor GFI1 plays critical roles  
264 in myeloid and lymphoid development and is an important pro-survival factor in T-ALL (Khandanpour et  
265 al., 2013, van der Meer, Jansen et al., 2010). The protein partnerships on which GFI1 depends for this role  
266 may offer potential therapeutic targets in T-ALL, but are as yet ill-defined. Here, using an unbiased  
267 quantitative proximity labeling approach, we identify GFI1 interacting proteins in T-ALL cells. Among  
268 these, IKAROS serves as a cooperating partner for GFI1-mediated gene regulation. Functional studies using  
269 T-ALL cells reveal a previously unrecognized role for GFI1 in transcriptional activation of genes that are  
270 among its targets, and several of which are involved in T cell development.

271 GFI1 and GFI1B have been largely described as transcriptional repressors, and indeed can  
272 substitute for one another *in vivo*. Repression requires a highly conserved 20-amino acid N-terminal SNAG  
273 domain capable of recruiting LSD1 complexed with CoREST (Saleque, Kim et al., 2007). In previous  
274 studies, point mutations or truncations in the SNAG domain that disrupt GFI1/1B—LSD1 binding impair  
275 GFI1/1B functions in multiple assays, pinpointing LSD1 as a central cofactor in GFI1/1B-mediated  
276 transcriptional repression and the establishment of downstream phenotypes (Grimes et al., 1996, McClellan  
277 et al., 2019, Saleque et al., 2007, Velinder et al., 2017). However, it is not clear whether GFI1/1B can  
278 regulate gene expression through other mechanisms, especially in cooperation with other factors. We  
279 applied BioID proximity labeling to identify GFI1-interacting proteins where the promiscuous biotin ligase  
280 (BirA\*) (Kim, Jensen et al., 2016, Roux, Kim et al., 2012) is fused to GFI1. Relative to co-  
281 immunoprecipitation, this method has the advantage that transient and indirect interactions can be  
282 efficiently captured. We utilized this method together with human CCRF-CEM T-ALL cells to  
283 systematically label proteins spatially close to GFI1, identifying GFI1 itself and some 500 direct or indirect  
284 interacting partners. Among these are previously identified GFI1-interacting proteins HMG20B, STAG1  
285 and components of the BHC complex including LSD1, CoREST, and GSE1. We segregated interacting  
286 proteins into functional groups and analyzed their network relationships. Through this analysis we

287 identified IKAROS, encoded by the *IKZF1* gene, as a top hit. IKAROS is also a zinc finger transcription  
288 factor that plays multiple, key roles in hematopoiesis, including in the development of B and T cells  
289 (Georgopoulos et al., 1994, Georgopoulos, Moore et al., 1992, Hahm, Ernst et al., 1994). As with GF11,  
290 IKAROS has also been linked to mouse and human T-ALL. In T-ALL, IKAROS functions as a tumor  
291 suppressor, and its deletion is a poor prognostic indicator for affected patients (Marcais, Jeannet et al., 2010,  
292 Sun, Crotty et al., 1999, Winandy, Wu et al., 1995). This impact on prognosis takes on a new dimension  
293 when considered in the context of the GF11—IKAROS partnership.

294 GF11 and IKAROS do not co-precipitate in conventional co-IP assays, suggesting their interaction  
295 is indirect and transient in nature. Biotin transfer between the two proteins depends on DNA binding but  
296 does not depend on the GF11 SNAG domain. Because GF11 and IKAROS are both sequence-specific DNA  
297 binding proteins, we performed ChIP-Seq to identify potential common target genes. This effort  
298 identified >25,000 GF11-bound and >50,000 IKAROS-bound peaks, and with considerable overlap. The  
299 large number of IKAROS peaks is consistent with previous reports for IKAROS binding in human K562  
300 and myeloma cell lines (Barwick, Neri et al., 2019, Consortium, 2012) and may be attributable to its ability  
301 to bind DNA in multimeric configurations (McCarty, Kleiger et al., 2003, Molnar, Wu et al., 1996).  
302 Approximately 80% (19966/25674) of GF11 bound peaks overlap with IKAROS peaks, supporting the idea  
303 that the two proteins frequently coregulate target gene expression. Co-occupied targets include *GF11* itself,  
304 as well as *NOTCH3*, the *CD3* gene cluster (*CD3E*, *CD3D* and *CD3G*), *TCF3*, *MYC*, *RUNX3*, *MYB* and  
305 *HES1*, each with fundamental roles in T-cell development. Interplay between GF11 and other transcription  
306 factors has been described. For example, GF11 and HOXA9 compete for overlapping binding sites at a  
307 distinct class of targets in AML (Velu, Chaubey et al., 2014). Unlike HOXA9, our results suggest that  
308 IKAROS cooperates with GF11.

309 RNA-Seq gene expression profiling using CCRF-CEM cells with ectopic GF11 expression and/or  
310 with IKAROS knockout revealed a group of genes positively regulated by both proteins. Among these  
311 genes are *NOTCH3* and *RAG1*, while other NOTCH family members *NOTCH1*, *NOTCH2*, and *NOTCH4*  
312 were not affected by enforced expression of GF11. This indicates *NOTCH3* is the specific NOTCH gene

313 targeted for induction by the GFII—IKAROS partnership. Moreover, genes making up this group are  
314 enriched for GFII and IKAROS occupancy, strongly suggesting they are direct targets and that the positive  
315 effects of the GFII—IKAROS partnership on transcription are also direct in nature.

316 In CCRF-CEM cells *NOTCH1*-activating mutation and *FBXW7* loss-of-function drive constitutive  
317 NOTCH signaling (O'Neil, Grim et al., 2007). Similarly, SUP-T1 cells carry a t(7;9) translocation driving  
318 expression of a truncated NOTCH variant to produce constitutive, ligand-independent NOTCH activity  
319 (Reynolds, Smith et al., 1987). Using both cell lines, we find that GFII and IKAROS promote NOTCH3  
320 cell surface expression. Moreover, mutations in the GFII SNAG domain that block the interaction with  
321 LSD1 also render GFII incapable of inducing NOTCH3. It is not clear whether LSD1 itself is important  
322 for this activation (e.g., through demethylating repressive protein modifications such as H3K9 methylation),  
323 or whether interactions between the SNAG domain and some other positively-acting cofactor become  
324 dominant in the case of GFII—IKAROS coregulated genes. Interestingly, SP-2509 and SNAG mutants,  
325 both of which disrupt GFII—LSD1 binding, yield qualitatively opposite results in NOTCH3 cell surface  
326 expression. Because SP-2509 leaves SNAG domain primary structure intact, our findings could indicate  
327 that LSD1 and an as yet unidentified co-activator compete for SNAG domain binding in an IKAROS-  
328 dependent manner. To address this possibility, we used lenalidomide to acutely abolish IKAROS expression.  
329 Lenalidomide is a thalidomide derivative that is active in multiple myeloma by enabling targeted  
330 degradation of IKAROS (Lu et al., 2014). We find that acute IKAROS depletion blunts GFII-mediated  
331 transactivation and cell surface expression of NOTCH3, consistent with GFII and IKAROS providing a  
332 platform for SNAG-dependent recruitment of a transcriptional co-activating principle, leading to  
333 transactivation of a gene expression program represented by the *NOTCH3* response.

334 Cumulatively, the results support a model in which the presence of IKAROS allows for activation  
335 of target genes by GFII. This model is consistent with the identification of SWI/SNF, a chromatin  
336 remodeling complex associated with positive regulation of gene expression (Hirschhorn, Brown et al., 1992,  
337 Imbalzano, Kwon et al., 1994, Kwon, Imbalzano et al., 1994, Peterson & Herskowitz, 1992), as a GFII  
338 proximity partner. An activating potential for both IKAROS and GFII has been described previously.

339 IKAROS binds and activates *Cd3d* through an upstream enhancer region (Georgopoulos et al., 1994,  
340 Georgopoulos et al., 1992). CD3 proteins form a central component of the T cell receptor signaling complex  
341 (Ngoenkam, Schamel et al., 2018). Positive regulation of gene expression by GFI1 was found in mouse  
342 granulocyte-monocyte precursor cells (GMPs) undergoing a binary monocyte/granulocyte fate decision. In  
343 GMPs it was shown that GFI1 associates with granulocyte-specific targets such as *Per3* and *Ets1*, activating  
344 their expression as part of a broader granulocyte fate-specifying program. Concurrently, GFI1 binding and  
345 repression of monocyte-specific genes suppresses the monocyte program (Olsson, Venkatasubramanian et  
346 al., 2016). It seems reasonable to consider that concurrent activation and repression of opposing gene  
347 expression programs, such as those exemplified by the GFI1—IKAROS—LSD1 relationship could direct  
348 alternative outcomes in developmental hematopoiesis. More work is necessary to define the molecular  
349 mechanisms by which GFI1 switches between repressive and activating transcriptional potential to control  
350 these binary fate decisions.



## 351 **Materials and Methods**

### 352 **Cells and Culture conditions**

353 CCRF-CEM and SUP-T1 cells were purchased from ATCC. Both cell lines were cultured in RPMI 1640  
354 medium, 10% fetal bovine serum, 2 mM GlutaMAX-I, 100 U/mL penicillin and 100 µg/mL streptomycin.  
355 All cell culture materials were purchased from ThermoFisher Scientific, Waltham, MA.

356

### 357 **Antibodies**

358 Antibodies used for immunoblotting and immunoprecipitation were as follows: anti-LSD1 (CST, C69G12,  
359 2184S); anti-CoREST (CST, D6I2U,14567S); anti-IKAROS (ThermoFisher Scientific, PA5-23728); anti-  
360 β-actin (Santa Cruz, C4, sc-47778); anti-α-tubulin (Santa Cruz, B-7, sc-5286); anti-FLAG (Sigma, M2,  
361 F1804); anti-HA antibody (Roche, 12CA5, 11583816001). Streptavidin-HRP was purchased from GE  
362 Healthcare (RPN1231).

363

### 364 **Constructs and Cloning**

365 In-frame GFII fusion proteins with BirA\* were created by subcloning GFII from constructs in our previous  
366 study (Velinder et al., 2017) into the *EcoRI* and *BamHI* sites of the MCS-BioID2-HA vector (a gift from  
367 Kyle Roux, Addgene #74224). Subsequently, GFII-BirA\*-HA PCR products were cloned into the *NotI* and  
368 *EcoRI* sites of the pLVX-Tight-Puro vector (Clontech Laboratories, Inc). We used the rat GFII ortholog  
369 for our experiments, which is >99% conserved at the amino acid level with human GFII. IKZF1/IKAROS  
370 constructs were based on the human form. The N383S derivative of rat GFII is analogous to the N382S  
371 mutation in human GFII.

372

### 373 **Lentivirus Packaging**

374 To generate lentiviral particles, HEK293T cells were transfected with lentiviral packaging vectors, viral  
375 packaging (psPAX2) and viral envelope (pMD2G) constructs at a 4:2:1 ratio with 1 mg/mL  
376 polyethylenimine (PEI, linear MD 25,000 Da, Sigma, Cat# 408727). The ratio of total transfected DNA to

377 PEI was 1:3 (1  $\mu$ g DNA:3  $\mu$ g PEI). After 24 hr, 20 mL of fresh cell culture medium was added and the cells  
378 were incubated for an additional 24 hr. Then the culture medium was replaced with virus collection medium  
379 (culture medium with 20mM HEPES). Viral supernatants were collected after a further 8 and 24hr. The two  
380 supernatants were combined and passed through a 0.45 $\mu$ m filter. Virus was directly used for infection or  
381 stored at -80°C.

382

### 383 **BioID proximity purification and proteomic analysis (MassIVE File Identifier MSV000086405)**

384 CCRF-CEM cells were transduced with Tet-On lentiviral vectors (Lenti-XTM Tet-On Advanced, Clontech  
385 Laboratories, Inc) and selected with 500  $\mu$ g/mL G418 to generate CCRF-CEM-Tet-On cells. CCRF-CEM-  
386 Tet-On cells were transduced with empty vector, BirA\*-HA or GFI1-BirA\*-HA viruses (pLVX-Tight-Puro,  
387 pLVX-Tight-puro-BirA\*-HA or pLVX-Tight-Puro-GFI1-BirA\*-HA, respectively) and selected with 0.5  
388  $\mu$ g/mL puromycin to generate CCRF-CEM cells expressing doxycycline-inducible GFI1-BirA\* fusion  
389 proteins or BirA\*. Cells were treated with 1  $\mu$ g/mL doxycycline for 48 hr and 20  $\mu$ M biotin for 16 hr. Cells  
390 were lysed in buffer (50 mM Tris-HCl pH 7.5, 500 mM NaCl, 0.5 mM EDTA, 1% Triton X-100) and  
391 incubated with streptavidin-Sepharose High Performance beads (Sigma, GE17-5113-01) on ice for 16hr.  
392 After washing the beads five times with lysis buffer on ice, proteins were eluted with 2 $\times$  Laemmli Sample  
393 Buffer (LSB, 65.8 mM Tris-HCl pH 6.8, 26.3% (w/v) glycerol, 2.1% SDS, 0.01% bromophenol blue) and  
394 boiled for 10 min. Proteins were resolved by SDS-PAGE. Whole lanes of SDS-PAGE gel were cut out and  
395 subjected to LTQ Orbitrap Velos Pro ion-trap mass spectrometry (ThermoFisher Scientific, Waltham, MA).  
396 Peptides were detected, isolated, and fragmented to produce a tandem mass spectrum of specific fragment  
397 ions for each peptide. Protein identity was determined by matching protein databases with the acquired  
398 fragmentation pattern by the software program, Sequest (ThermoFisher Scientific, Waltham, MA). All  
399 databases include a reversed version of all the sequences and the data was filtered to a 1-2% peptide false  
400 discovery rate.

401

402 **ChIP-Seq (Gene Expression Omnibus Series record GSE160183)**

403 The CCRF-CEM-Tet-On cells described above were infected with GF11-3×FLAG or IKAROS-3×FLAG  
404 viruses (packaged with pLVX-Tight-puro-GF11-3×FLAG or pLVX-Tight-puro-IKAROS-3×FLAG  
405 plasmids). Cells were selected with 1µg/mL puromycin to produce CCRF-CEM stable cell lines inducibly  
406 expressing GF11-3×FLAG and IKAROS-3×FLAG. These cells were treated with 1µg/mL doxycycline for  
407 24 hr. 20 million CCRF-CEM cells were crosslinked using a final concentration of 1% formaldehyde in the  
408 medium for 10 min. Crosslinking was quenched with 0.125 M glycine for 2 min. Cells were washed with  
409 ice-cold PBS and Farnham lysis buffer (5 mM PIPES pH 8.0, 85 mM KCl, 0.5% NP-40, 1 mM PMSF and  
410 10µg/mL Aprotinin pH 8.0). Cells were resuspended in 1 mL RIPA lysis buffer (1X PBS, 1% NP-40, 0.5%  
411 sodium deoxycholate, 0.1% SDS, 1 mM PMSF and 10 µg/mL Aprotinin pH 8.0). Cells were sonicated to  
412 shear the DNA to between 200 and 500 bp. Fifty µL of sonicated chromatin was saved. The leftover samples  
413 were precipitated with anti-FLAG antibody which was prebound to Protein G Dynabeads (Thermo Fisher).  
414 The 50 µL of saved chromatin and immunoprecipitated DNA were de-crosslinked in a 65°C water bath  
415 overnight. De-crosslinked samples were purified using a Zymo ChIP DNA clean & concentrator (Zymo  
416 Research). Five to 10 ng of precipitated DNA was used for library construction using NEBNext ChIP-Seq  
417 Library Prep Reagent Set. Sequencing libraries (25 pM) were chemically denatured and applied to an  
418 Illumina HiSeq v4 single read flow cell using an Illumina cBot. Hybridized molecules were clonally  
419 amplified and annealed to sequencing primers with reagents from an Illumina HiSeq SR Cluster Kit v4-  
420 cBot (GD-401-4001). Following transfer of the flow cell to an Illumina HiSeq 2500 instrument  
421 (HCSv2.2.38 and RTA v1.18.61), a 50-cycle single-read sequence run was performed using HiSeq SBS Kit  
422 v4 sequencing reagents (FC-401-4002).

423

424 **ChIP-Seq analysis**

425 SAM alignments were generated from Illumina Fastq files aligned to human hg38 genome using  
426 Novocraft's novoalign aligner (<http://www.novocraft.com>) with the following parameters: -o SAM -r

427 Random. Peak calling was then performed using macs2 (<https://github.com/taoliu/MACS>, v2.1.1.20160309)  
428 with the following settings: -g 2.7e9 -call -summit -f BAMPE -nomodel -B -SPMR -extsize 200.  
429 Generated bedgraph files were then transformed to bw format using UCSC bedGraphToBigWig application  
430 (v4). Heatmap clustering of ChIP-SEQ was carried out using deepTools (v3). Matrix was generated with  
431 computeMatrix application using the following parameters: computeMatrix -S input\_1.bw input\_2.bw -R  
432 peaks.bed -outFileName out.matrix -referencePoint center -a 10000 -b 10000 -bs 100 -sortRegions descend.  
433 Correlation heatmap was generated using the deep Tools plot Heatmap application. PCA analysis was  
434 performed using the deepTools plotPCA application. The peaks.bed was generated by combining peaks  
435 from two ChIP-Seq experiments. plotHeatmap application with default settings was then used to plot  
436 heatmap. Peak regions were further used for motif finding analysis, which was carried out using the  
437 findMotifGenome.pl application (v4.8.3, HOMER, <http://homer.ucsd.edu/homer/motif/>) with default  
438 settings. This resulted in between 92.6M and 86.4M reads, wherein between 81.8M and 73.6M (88.3 and  
439 85.2%) uniquely mapped to the *Hg38* genome build.

440

#### 441 ***IKAROS/IKZF1* knockout**

442 Nonspecific or *IKZF1*-specific CRISPR/Cas9 RNPs were generated from tracrRNA-ATTO550 (IDT),  
443 crRNA (IDT) and Cas9 protein (QB3 MacroLab, UC Berkeley) using commercial guidelines (IDT) and  
444 transfected into GF11-3×FLAG CCRF-CEM cells by electroporation using the Neon transfection system  
445 10 µL kit (ThermoFisher Scientific). Electroporation parameters were 1500V, 10 ms pulse width, 3 pulses.  
446 Transfection efficiency was measured by flow cytometry to detect the tracrRNA-ATTO550 positive cells.  
447 Approximately 95% transfection efficiency was obtained. Cells were cultured for >9 days to confirm stable  
448 ablation of IKAROS protein by Western blotting. CRISPR guide RNAs were chosen targeting the 5' exons  
449 of the *IKZF1* gene using the IDT predesigned CRISPR guide RNA database  
450 ([https://www.idtdna.com/site/order/designtool/index/CRISPR\\_PREDESIGN](https://www.idtdna.com/site/order/designtool/index/CRISPR_PREDESIGN)): *IKAROS/IKZF1*:

451 TCATCTGGAGTATCGCTTACagg;

GACCTCTCCACCACCTCGGGagg;

452 CTCCAAGAGTGACAGAGTCGtg. CRISPR/Cas9 negative control crRNA (IDT, 1072544) was used as  
453 a control for transfection.

454

#### 455 **RNA-Seq (Gene Expression Omnibus Series record GSE160183)**

456 Total RNA was extracted from GF11-3×FLAG CCRF-CEM cells treated with or without doxycycline for  
457 24 hr, and with IKAROS or control CRISPR RNP knockout using the RNeasy Mini kit (Qiagen) and RNase-  
458 Free DNase Set (Qiagen). RNA integrity numbers (RIN) ranged from 9.4 to 9.9. Poly(A) RNA was purified  
459 from total RNA samples (100-500 ng) with oligo(dT) magnetic beads followed by library construction  
460 using the Illumina TruSeq Stranded mRNA Library Prep kit and TruSeq RNA UD Indexes. Purified  
461 libraries were qualified on an Agilent Technologies 2200 TapeStation using a D1000 ScreenTape assay.  
462 The molarity of adapter-modified molecules was defined by quantitative PCR using the Kapa Biosystems  
463 Kapa Library Quant Kit. Individual libraries were normalized to 1.30 nM in preparation for Illumina  
464 sequence analysis. NovaSeq 2×50 bp Sequencing\_100 M Read-Pairs Sequencing libraries (1.3 nM) were  
465 chemically denatured and applied to an Illumina NovaSeq flow cell using the NovaSeq XP chemistry  
466 workflow. Following transfer of the flowcell to an Illumina NovaSeq instrument, a 2×51 cycle paired-end  
467 sequence run was performed using a NovaSeq S1 reagent Kit.

468

#### 469 **RNA-seq analysis**

470 Filtering and alignments were performed using the analysis pipeline developed by the Huntsman Cancer  
471 Institute (HCI) Bioinformatic Core Facility  
472 ([https://huntsmancancerinstitute.github.io/hciRscripts/hciR\\_scripts.html](https://huntsmancancerinstitute.github.io/hciRscripts/hciR_scripts.html)). Briefly, fastq files were aligned  
473 using STAR aligned (v2.7.3a) with the following settings: --twopassMode Basic --outSAMtype BAM  
474 SortedByCoordinate --limitBAMsortRAM 6400000000 --outBAMsortingBinsN 100

475 --quantMode TranscriptomeSAM --outWigType bedGraph --outWigStrand Unstranded. The count matrix  
476 was then calculated using the Subread FeatureCounts function (v1.6.3) DESeq2 (v1.28.1) was used for  
477 differentially expressed genes analysis.

478

#### 479 ***In vitro* SNAG—LSD1 binding assay**

480 Biotinylated, lysine(K)-8 dimethylated SNAG peptide (Bio-K8me2-SNAG) was commercially synthesized  
481 and deployed as previously described in CCRF-CEM extracts in either the absence or presence of SP-2509  
482 (Velinder et al., 2017). Biotinylated peptides were collected on streptavidin-Sepharose beads whose non-  
483 specific binding sites were blocked in 1% bovine serum albumin (BSA) in 1X phosphate buffered saline  
484 (PBS). LSD1 was detected by western blotting in pellets and supernatants.

485

#### 486 **Data Availability**

487 ChIP-Seq and RNA-Seq datasets are available at the Gene Expression Omnibus (GEO) website  
488 <https://www.ncbi.nlm.nih.gov/geo/query/acc.cgi?acc=GSE160183>. The following secure token has been  
489 created to allow reviewer access of the data while it remains in private status: gjrcyuifxgxfaf. Should the  
490 manuscript be accepted for publication, the authors will direct GEO to release the data publicly. BioID  
491 mass spectrometry data were submitted to MassIVE with MassIVE File Identifier MSV000086405 at  
492 website: [https://massive.ucsd.edu/ProteoSAFe/private-](https://massive.ucsd.edu/ProteoSAFe/private-dataset.jsp?task=ff3728eabdb84663981aafe4e44df11b)  
493 [dataset.jsp?task=ff3728eabdb84663981aafe4e44df11b](https://massive.ucsd.edu/ProteoSAFe/private-dataset.jsp?task=ff3728eabdb84663981aafe4e44df11b). The data is still in private status. The following  
494 reviewer login credentials will allow reviewers to access. Username :MSV000086405\_reviewer; password:  
495 a.

496

#### 497 **Acknowledgements**

498 We thank F. Gounari and P. Ernst for critical reading of the manuscript. DNA sequencing and DNA  
499 oligonucleotides were synthesized by the University of Utah Health Sciences Center DNA/Peptide  
500 Synthesis Facility. We thank R. Tomaino at Taplin Mass Spectrometry Facility, Cell Biology Department,

501 Harvard Medical School for assistance with LS-MS/MS and analysis. CHIP-Seq and RNA-Seq data  
502 reported in this study utilized the University of Utah Huntsman Cancer Institute High-Throughput  
503 Genomics and Bioinformatic Analysis Shared Resources. We thank C. Stubben at the Huntsman Cancer  
504 Institute Bioinformatics Shared Resource for assistance with submitting NGS sequencing data to GEO, and  
505 S.M. Osburn at the University Mass Spectrometry Facility for assistance with submitting mass spectrometry  
506 data to MassIVE.

507

#### 508 **Author contributions**

509 WS, DM, DB, AP and MC performed the experiments analyzed the data. JG analyzed CHIP-Seq and RNA-  
510 Seq data. MEE and DT conceived and supervised the study and interpreted data. BRC provided technical  
511 support. All authors were involved in the writing of the manuscript.

512

#### 513 **Funding**

514 This work was supported by a National Institutes of Health Cancer Center Support Grant [P30CA042014],  
515 National Institutes of Health grants [R01CA201235] to MEE, [R01GM122778, R01AI100873] to DT and  
516 grants to MEE from American Cancer Society and Alex's Lemonade Stand Foundation.

517

#### 518 **Conflict of interest**

519 The authors declare no conflicts of interest, direct or indirect, associated with this manuscript.

520 **References**

- 521 Barwick BG, Neri P, Bahlis NJ, Nooka AK, Dhodapkar MV, Jaye DL, Hofmeister CC, Kaufman JL, Gupta  
522 VA, Auclair D, Keats JJ, Lonial S, Vertino PM, Boise LH (2019) Multiple myeloma immunoglobulin  
523 lambda translocations portend poor prognosis. *Nat Commun* 10: 1911
- 524 Bellavia D, Campese AF, Alesse E, Vacca A, Felli MP, Balestri A, Stoppacciaro A, Tiveron C, Tatangelo  
525 L, Giovarelli M, Gaetano C, Ruco L, Hoffman ES, Hayday AC, Lendahl U, Frati L, Gulino A, Screpanti I  
526 (2000) Constitutive activation of NF-kappaB and T-cell leukemia/lymphoma in Notch3 transgenic mice.  
527 *EMBO J* 19: 3337-48
- 528 Bellavia D, Campese AF, Checquolo S, Balestri A, Biondi A, Cazzaniga G, Lendahl U, Fehling HJ, Hayday  
529 AC, Frati L, von Boehmer H, Gulino A, Screpanti I (2002) Combined expression of pTalpha and Notch3  
530 in T cell leukemia identifies the requirement of preTCR for leukemogenesis. *Proc Natl Acad Sci U S A* 99:  
531 3788-93
- 532 Bernasconi-Elias P, Hu T, Jenkins D, Firestone B, Gans S, Kurth E, Capodiceci P, Deplazes-Lauber J,  
533 Petropoulos K, Thiel P, Ponsel D, Hee Choi S, LeMotte P, London A, Goetschkes M, Nolin E, Jones MD,  
534 Slocum K, Kluk MJ, Weinstock DM et al. (2016) Characterization of activating mutations of NOTCH3 in  
535 T-cell acute lymphoblastic leukemia and anti-leukemic activity of NOTCH3 inhibitory antibodies.  
536 *Oncogene* 35: 6077-6086
- 537 Choi SH, Severson E, Pear WS, Liu XS, Aster JC, Blacklow SC (2017) The common oncogenomic program  
538 of NOTCH1 and NOTCH3 signaling in T-cell acute lymphoblastic leukemia. *PLoS One* 12: e0185762
- 539 Consortium EP (2012) An integrated encyclopedia of DNA elements in the human genome. *Nature* 489:  
540 57-74
- 541 Coustan-Smith E, Mullighan CG, Onciu M, Behm FG, Raimondi SC, Pei D, Cheng C, Su X, Rubnitz JE,  
542 Basso G, Biondi A, Pui CH, Downing JR, Campana D (2009) Early T-cell precursor leukaemia: a subtype  
543 of very high-risk acute lymphoblastic leukaemia. *Lancet Oncol* 10: 147-56
- 544 Ferrando A (2010) NOTCH mutations as prognostic markers in T-ALL. *Leukemia* 24: 2003-4



545 Fiskus W, Sharma S, Shah B, Portier BP, Devaraj SGT, Liu K, Iyer SP, Bearss D, Bhalla KN (2017) Highly  
546 effective combination of LSD1 (KDM1A) antagonist and pan-histone deacetylase inhibitor against human  
547 AML cells. *Leukemia* 31: 1658

548 Georgopoulos K, Bigby M, Wang JH, Molnar A, Wu P, Winandy S, Sharpe A (1994) The Ikaros gene is  
549 required for the development of all lymphoid lineages. *Cell* 79: 143-56

550 Georgopoulos K, Moore DD, Derfler B (1992) Ikaros, an early lymphoid-specific transcription factor and  
551 a putative mediator for T cell commitment. *Science* 258: 808-12

552 Golde TE, Koo EH, Felsenstein KM, Osborne BA, Miele L (2013) gamma-Secretase inhibitors and  
553 modulators. *Biochim Biophys Acta* 1828: 2898-907

554 Grimes HL, Chan TO, Zweidler-McKay PA, Tong B, Tschlis PN (1996) The Gfi-1 proto-oncoprotein  
555 contains a novel transcriptional repressor domain, SNAG, and inhibits G1 arrest induced by interleukin-2  
556 withdrawal. *Mol Cell Biol* 16: 6263-72

557 Hahm K, Ernst P, Lo K, Kim GS, Turck C, Smale ST (1994) The lymphoid transcription factor LyF-1 is  
558 encoded by specific, alternatively spliced mRNAs derived from the Ikaros gene. *Mol Cell Biol* 14: 7111-  
559 23

560 Hirschhorn JN, Brown SA, Clark CD, Winston F (1992) Evidence that SNF2/SWI2 and SNF5 activate  
561 transcription in yeast by altering chromatin structure. *Genes Dev* 6: 2288-98

562 Hock H, Hamblen MJ, Rooke HM, Schindler JW, Saleque S, Fujiwara Y, Orkin SH (2004) Gfi-1 restricts  
563 proliferation and preserves functional integrity of haematopoietic stem cells. *Nature* 431: 1002-7

564 Hock H, Hamblen MJ, Rooke HM, Traver D, Bronson RT, Cameron S, Orkin SH (2003) Intrinsic  
565 requirement for zinc finger transcription factor Gfi-1 in neutrophil differentiation. *Immunity* 18: 109-20

566 Hones JM, Botezatu L, Helness A, Vadnais C, Vassen L, Robert F, Hergenhan SM, Thivakaran A, Schutte  
567 J, Al-Matary YS, Lams RF, Fraszczak J, Makishima H, Radivoyevitch T, Przychodzen B, da Conceicao  
568 Castro SV, Gorgens A, Giebel B, Klein-Hitpass L, Lennartz K et al. (2016) GFI1 as a novel prognostic and  
569 therapeutic factor for AML/MDS. *Leukemia* 30: 1237-45

570 Imbalzano AN, Kwon H, Green MR, Kingston RE (1994) Facilitated binding of TATA-binding protein to  
571 nucleosomal DNA. *Nature* 370: 481-5

572 Inui K, Zhao Z, Yuan J, Jayaprakash S, Le LTM, Drakulic S, Sander B, Golas MM (2017) Stepwise  
573 assembly of functional C-terminal REST/NRSF transcriptional repressor complexes as a drug target.  
574 *Protein Sci* 26: 997-1011

575 Karsunky H, Zeng H, Schmidt T, Zevnik B, Kluge R, Schmid KW, Duhren U, Moroy T (2002)  
576 Inflammatory reactions and severe neutropenia in mice lacking the transcriptional repressor Gfi1. *Nat Genet*  
577 30: 295-300

578 Khandanpour C, Krongold J, Schutte J, Bouwman F, Vassen L, Gaudreau MC, Chen R, Calero-Nieto FJ,  
579 Diamanti E, Hannah R, Meyer SE, Grimes HL, van der Reijden BA, Jansen JH, Patel CV, Peeters JK,  
580 Lowenberg B, Duhren U, Gottgens B, Moroy T (2012) The human GF1136N variant induces epigenetic  
581 changes at the Hoxa9 locus and accelerates K-RAS driven myeloproliferative disorder in mice. *Blood* 120:  
582 4006-17

583 Khandanpour C, Phelan JD, Vassen L, Schutte J, Chen R, Horman SR, Gaudreau MC, Krongold J, Zhu J,  
584 Paul WE, Duhren U, Gottgens B, Grimes HL, Moroy T (2013) Growth factor independence 1 antagonizes  
585 a p53-induced DNA damage response pathway in lymphoblastic leukemia. *Cancer Cell* 23: 200-14

586 Kim DI, Jensen SC, Noble KA, Kc B, Roux KH, Motamedchaboki K, Roux KJ (2016) An improved smaller  
587 biotin ligase for BioID proximity labeling. *Mol Biol Cell* 27: 1188-96

588 Kuehn HS, Boisson B, Cunningham-Rundles C, Reichenbach J, Stray-Pedersen A, Gelfand EW, Maffucci  
589 P, Pierce KR, Abbott JK, Voelkerding KV, South ST, Augustine NH, Bush JS, Dolen WK, Wray BB, Itan  
590 Y, Cobat A, Sorte HS, Ganesan S, Prader S et al. (2016) Loss of B Cells in Patients with Heterozygous  
591 Mutations in IKAROS. *N Engl J Med* 374: 1032-1043

592 Kwon H, Imbalzano AN, Khavari PA, Kingston RE, Green MR (1994) Nucleosome disruption and  
593 enhancement of activator binding by a human SW1/SNF complex. *Nature* 370: 477-81

594 Lu G, Middleton RE, Sun H, Naniong M, Ott CJ, Mitsiades CS, Wong KK, Bradner JE, Kaelin WG, Jr.  
595 (2014) The myeloma drug lenalidomide promotes the cereblon-dependent destruction of Ikaros proteins.  
596 *Science* 343: 305-9

597 Maiques-Diaz A, Spencer GJ, Lynch JT, Ciceri F, Williams EL, Amaral FMR, Wiseman DH, Harris WJ,  
598 Li Y, Sahoo S, Hitchin JR, Mould DP, Fairweather EE, Waszkowycz B, Jordan AM, Smith DL, Somerville  
599 TCP (2018) Enhancer Activation by Pharmacologic Displacement of LSD1 from GF11 Induces  
600 Differentiation in Acute Myeloid Leukemia. *Cell Rep* 22: 3641-3659

601 Marçais A, Jeannet R, Hernandez L, Soulier J, Sigaux F, Chan S, Kastner P (2010) Genetic inactivation of  
602 Ikaros is a rare event in human T-ALL. *Leuk Res* 34: 426-9

603 McCarty AS, Kleiger G, Eisenberg D, Smale ST (2003) Selective dimerization of a C2H2 zinc finger  
604 subfamily. *Mol Cell* 11: 459-70

605 McClellan D, Casey MJ, Bareyan D, Lucente H, Ours C, Velinder M, Singer J, Lone MD, Sun W, Coria Y,  
606 Mason CC, Engel ME (2019) Growth Factor Independence 1B-Mediated Transcriptional Repression and  
607 Lineage Allocation Require Lysine-Specific Demethylase 1-Dependent Recruitment of the BHC Complex.  
608 *Mol Cell Biol* 39

609 Molnar A, Wu P, Largespada DA, Vortkamp A, Scherer S, Copeland NG, Jenkins NA, Bruns G,  
610 Georgopoulos K (1996) The Ikaros gene encodes a family of lymphocyte-restricted zinc finger DNA  
611 binding proteins, highly conserved in human and mouse. *J Immunol* 156: 585-92

612 Ngoenkam J, Schamel WW, Pongcharoen S (2018) Selected signalling proteins recruited to the T-cell  
613 receptor-CD3 complex. *Immunology* 153: 42-50

614 O'Neil J, Grim J, Strack P, Rao S, Tibbitts D, Winter C, Hardwick J, Welcker M, Meijerink JP, Pieters R,  
615 Draetta G, Sears R, Clurman BE, Look AT (2007) FBW7 mutations in leukemic cells mediate NOTCH  
616 pathway activation and resistance to gamma-secretase inhibitors. *J Exp Med* 204: 1813-24

617 Olsson A, Venkatasubramanian M, Chaudhri VK, Aronow BJ, Salomonis N, Singh H, Grimes HL (2016)  
618 Single-cell analysis of mixed-lineage states leading to a binary cell fate choice. *Nature* 537: 698-702

619 Person RE, Li FQ, Duan Z, Benson KF, Wechsler J, Papadaki HA, Eliopoulos G, Kaufman C, Bertolone  
620 SJ, Nakamoto B, Papayannopoulou T, Grimes HL, Horwitz M (2003) Mutations in proto-oncogene GFI1  
621 cause human neutropenia and target ELA2. *Nat Genet* 34: 308-12

622 Peterson CL, Herskowitz I (1992) Characterization of the yeast SWI1, SWI2, and SWI3 genes, which  
623 encode a global activator of transcription. *Cell* 68: 573-83

624 Quentmeier H, Pommerenke C, Dirks WG, Eberth S, Koeppel M, MacLeod RAF, Nagel S, Steube K,  
625 Uphoff CC, Drexler HG (2019) The LL-100 panel: 100 cell lines for blood cancer studies. *Sci Rep* 9: 8218

626 Reynolds TC, Smith SD, Sklar J (1987) Analysis of DNA surrounding the breakpoints of chromosomal  
627 translocations involving the beta T cell receptor gene in human lymphoblastic neoplasms. *Cell* 50: 107-17

628 Rothenberg EV, Taghon T (2005) Molecular genetics of T cell development. *Annu Rev Immunol* 23: 601-  
629 49

630 Roux KJ, Kim DI, Raida M, Burke B (2012) A promiscuous biotin ligase fusion protein identifies proximal  
631 and interacting proteins in mammalian cells. *J Cell Biol* 196: 801-10

632 Saleque S, Kim J, Rooke HM, Orkin SH (2007) Epigenetic regulation of hematopoietic differentiation by  
633 Gfi-1 and Gfi-1b is mediated by the cofactors CoREST and LSD1. *Mol Cell* 27: 562-72

634 Shi LZ, Kalupahana NS, Turnis ME, Neale G, Hock H, Vignali DA, Chi H (2013) Inhibitory role of the  
635 transcription repressor Gfi1 in the generation of thymus-derived regulatory T cells. *Proc Natl Acad Sci U*  
636 *S A* 110: E3198-205

637 Sun L, Crotty ML, Sensel M, Sather H, Navara C, Nachman J, Steinherz PG, Gaynon PS, Seibel N, Mao  
638 C, Vassilev A, Reaman GH, Uckun FM (1999) Expression of dominant-negative Ikaros isoforms in T-cell  
639 acute lymphoblastic leukemia. *Clin Cancer Res* 5: 2112-20

640 Szklarczyk D, Gable AL, Lyon D, Junge A, Wyder S, Huerta-Cepas J, Simonovic M, Doncheva NT, Morris  
641 JH, Bork P, Jensen LJ, Mering CV (2019) STRING v11: protein-protein association networks with  
642 increased coverage, supporting functional discovery in genome-wide experimental datasets. *Nucleic Acids*  
643 *Res* 47: D607-D613

644 Terwilliger T, Abdul-Hay M (2017) Acute lymphoblastic leukemia: a comprehensive review and 2017  
645 update. *Blood Cancer J* 7: e577

646 Tinsley KW, Hong C, Luckey MA, Park JY, Kim GY, Yoon HW, Keller HR, Sacks AJ, Feigenbaum L,  
647 Park JH (2013) Ikaros is required to survive positive selection and to maintain clonal diversity during T-  
648 cell development in the thymus. *Blood* 122: 2358-68

649 Tottone L, Zhdanovskaya N, Carmona Pestana A, Zampieri M, Simeoni F, Lazzari S, Ruocco V, Pelullo  
650 M, Caiafa P, Felli MP, Checquolo S, Bellavia D, Talora C, Screpanti I, Palermo R (2019) Histone  
651 Modifications Drive Aberrant Notch3 Expression/Activity and Growth in T-ALL. *Front Oncol* 9: 198

652 van der Meer LT, Jansen JH, van der Reijden BA (2010) Gfi1 and Gfi1b: key regulators of hematopoiesis.  
653 *Leukemia* 24: 1834-43

654 Velinder M, Singer J, Bareyan D, Meznarich J, Tracy CM, Fulcher JM, McClellan D, Lucente H, Franklin  
655 S, Sharma S, Engel ME (2017) GFI1 functions in transcriptional control and cell fate determination require  
656 SNAG domain methylation to recruit LSD1. *Biochem J* 474: 2951

657 Velu CS, Chaubey A, Phelan JD, Horman SR, Wunderlich M, Guzman ML, Jegga AG, Zeleznik-Le NJ,  
658 Chen J, Mulloy JC, Cancelas JA, Jordan CT, Aronow BJ, Marcucci G, Bhat B, Gebelein B, Grimes HL  
659 (2014) Therapeutic antagonists of microRNAs deplete leukemia-initiating cell activity. *J Clin Invest* 124:  
660 222-36

661 Volpe G, Walton DS, Grainger DE, Ward C, Cauchy P, Blakemore D, Coleman DJL, Cockerill PN, Garcia  
662 P, Frampton J (2017) Prognostic significance of high GFI1 expression in AML of normal karyotype and its  
663 association with a FLT3-ITD signature. *Sci Rep* 7: 11148

664 Waegemans E, Van de Walle I, De Medts J, De Smedt M, Kerre T, Vandekerckhove B, Leclercq G, Wang  
665 T, Plum J, Taghon T (2014) Notch3 activation is sufficient but not required for inducing human T-lineage  
666 specification. *J Immunol* 193: 5997-6004

667 Winandy S, Wu P, Georgopoulos K (1995) A dominant mutation in the Ikaros gene leads to rapid  
668 development of leukemia and lymphoma. *Cell* 83: 289-99

669 Xu X, Choi SH, Hu T, Tiyanont K, Habets R, Groot AJ, Vooijs M, Aster JC, Chopra R, Fryer C, Blacklow  
670 SC (2015) Insights into Autoregulation of Notch3 from Structural and Functional Studies of Its Negative  
671 Regulatory Region. *Structure* 23: 1227-35

672 Yucel R, Karsunky H, Klein-Hitpass L, Moroy T (2003) The transcriptional repressor Gfi1 affects  
673 development of early, uncommitted c-Kit<sup>+</sup> T cell progenitors and CD4/CD8 lineage decision in the thymus.  
674 *J Exp Med* 197: 831-44

675 Zarebski A, Velu CS, Baktula AM, Bourdeau T, Horman SR, Basu S, Bertolone SJ, Horwitz M, Hildeman  
676 DA, Trent JO, Grimes HL (2008) Mutations in growth factor independent-1 associated with human  
677 neutropenia block murine granulopoiesis through colony stimulating factor-1. *Immunity* 28: 370-80

678 Zeng H, Yucel R, Kosan C, Klein-Hitpass L, Moroy T (2004) Transcription factor Gfi1 regulates self-  
679 renewal and engraftment of hematopoietic stem cells. *EMBO J* 23: 4116-25

680 Zhang J, Ding L, Holmfeldt L, Wu G, Heatley SL, Payne-Turner D, Easton J, Chen X, Wang J, Rusch M,  
681 Lu C, Chen SC, Wei L, Collins-Underwood JR, Ma J, Roberts KG, Pounds SB, Ulyanov A, Becksfort J,  
682 Gupta P et al. (2012) The genetic basis of early T-cell precursor acute lymphoblastic leukaemia. *Nature*  
683 481: 157-63

684 Zhang J, Jackson AF, Naito T, Dose M, Seavitt J, Liu F, Heller EJ, Kashiwagi M, Yoshida T, Gounari F,  
685 Petrie HT, Georgopoulos K (2011) Harnessing of the nucleosome-remodeling-deacetylase complex  
686 controls lymphocyte development and prevents leukemogenesis. *Nat Immunol* 13: 86-94

687

688 **Figure legends**

689 **Figure 1.** BioID proximity labeling identifies GFII-interacting proteins. **(A)** Scheme for BioID proximity  
690 labeling method to identify GFII-proximate proteins. Gray circle reflects the radius for biotinylation of  
691 nearby molecules such as GFII itself and its known binding partner LSD1, as well as unknown proteins A,  
692 B and C but not D. **(B)** CCRF-CEM cells inducibly express BirA\*-HA alone or as a fusion with GFII.  
693 Biotin-treated CCRF-CEM cells transduced with empty vector (lanes 1-2), BirA\*-HA (lanes 3-4), or GFII-  
694 BirA\*-HA (lanes 5-6) were treated with doxycycline (Doxy) (+) or vehicle control (-). Whole cell lysates  
695 (WCL) were resolved by SDS-PAGE and immunoblotted using HA antibodies.  $\alpha$ -tubulin is shown as a  
696 loading control. **(C)** Biotinylation of GFII-associated proteins LSD1 and CoREST is enriched using GFII-  
697 BirA\*-HA expressing CCRF-CEM cells relative to empty vector or BirA\*-HA controls. Whole cell lysates  
698 prepared as in (B) were used for immunoblotting or were first precipitated using streptavidin Sepharose  
699 beads (SAv-P), and subsequently analyzed by immunoblotting with anti-HA, anti-LSD1 or anti-CoREST  
700 antibodies, or streptavidin-HRP (SAv:HRP) to detect biotinylation.

701

702 **Figure 2.** Top hits of GFII proximal partners identified by proteome-wide BioID labeling. **(A)** Volcano  
703 plot of proteins identified by BioID proximity labeling. Thresholds (red dashed lines) were fold-  
704 difference  $>2$  and  $P$ -value  $<0.05$ . **(Inset)** Magnified portion of (A) depicting significant hits. Known GFII  
705 partners and GFII itself are labeled in red. **(B)** Genes labeled in (A) were subjected to STRING (version  
706 10.5) functional protein association network analysis. Edges represent protein—protein associations. Blue  
707 indicates annotated nuclear proteins. Red indicates annotated proteins associated with gene regulation. The  
708 network was clustered using the MCL algorithm with inflation parameter 3. Dotted line indicates the  
709 proteins belong to different clusters.

710

711 **Figure 3.** The GFII—IKAROS interaction requires DNA binding. **(A)** Validation and non-LSD1 binding  
712 dependence of the GFII—IKAROS proximity relationship. Biotinylated proteins in whole cell lysates from  
713 CCRF-CEM cells transduced with the indicated constructs and treated as in Figure 1B were isolated with

714 streptavidin beads and immunoblotted with anti-IKAROS and anti-HA antibodies targeting the epitope tag  
715 in GFII-BirA\* fusion protein variants. **(B)** GFII—IKAROS binding is not observed in traditional  
716 coprecipitation methods. Lysates from CCRF-CEM cells inducibly expressing wild type GFII-3×FLAG or  
717 variants (K8L,P2A and ΔSNAG) were immunoprecipitated with anti-FLAG antibody and Protein G-  
718 Sepharose. The presence or absence of IKAROS, CoREST, or GFII in the precipitate was detected by  
719 immunoblotting with anti-IKAROS, anti-CoREST or anti-FLAG antibodies. 2% input whole cell lysate  
720 (WCL) is shown as a control. **(C)** The proximity relationship between GFII and IKAROS requires DNA  
721 binding activity of both proteins. HEK293T cells were transiently transfected with empty vector or GFII-  
722 BirA\*-HA (wild type or N383S) together with human IKAROS-3×FLAG (wild type or N159A) expression  
723 constructs. IKAROS and control GFII biotinylation was monitored by precipitation with streptavidin beads  
724 and IKAROS immunoblotting as described in panel A. A GFII immunoblot is shown to confirm equivalent  
725 precipitation with streptavidin-Sepharose beads.

726

727 **Figure 4.** Identification of GFII and IKAROS targets in CCRF-CEM cells. **(A)** Validation of GFII and  
728 IKAROS expression in CCRF-CEM cell lines by Western blotting. CCRF-CEM cells expressing GFII-  
729 3×FLAG and IKAROS-3×FLAG were used for ChIP-Seq. **(B)** Venn diagram showing enumeration of  
730 unique and shared GFII and IKAROS ChIP-Seq peaks. **(C)** Left: GFII ChIP-Seq heatmap showing all peak  
731 sites, centered by the ChIP peak summit and arranged from strongest to weakest. Right: the same set of  
732 peak summits in the same order shown as an IKAROS binding heatmap. **(D)** Example Integrative Genomics  
733 Viewer (IGV) tracks of GFII ChIP-Seq and input controls (purple), IKAROS ChIP-Seq and input controls  
734 (teal), together with previously published RNA-Seq (peach) of CCRF-CEM cells. *NOTCH3*, *GFII*, *MYC*,  
735 *MYB*, *CD3*, *HES1*, *RUNX3* and *TCF3* tracks are shown.

736

737 **Figure 5.** GFII and IKAROS positively regulate a subset of target genes. **(A)** IKAROS Western blot of  
738 untransfected CCRF-CEM-GFII-3×FLAG cells, cells electroporated with ATTO550-conjugated control or



739 IKAROS-specific RNPs. 24 hr post-transfection, ATTO550<sup>+</sup> cells were sorted and cultured for 9 additional  
740 days prior to preparation of lysates.  $\beta$ -actin is shown as a loading control. **(B)** RNA-Seq analysis was  
741 performed using the same control RNP- or IKAROS-specific RNP-transfected cells shown in (A) after  
742 treatment with vehicle or doxycycline (Doxy) for 24 hr. The top 500 differentially expressed genes (based  
743 on *P*-value) were subjected to hierarchical clustering and are shown as a heatmap. Gene groupings with  
744 distinct expression patterns (1-5) are highlighted. **(C)** IGV tracks displaying GFI1 and IKAROS ChIP-Seq  
745 and RNA-Seq read distribution for *NOTCH3*.

746

747 **Figure 6.** IKAROS cooperates with GFI1 to regulate cell surface NOTCH3 protein expression. **(A)** Left:  
748 example flow cytometry histograms showing NOTCH3 surface expression in CCRF-CEM-GFI1-3 $\times$ FLAG  
749 cells treated with doxycycline (Doxy) for the indicated times. Untreated (0 hr) cells are shown as a control.  
750 Right: NOTCH3 MFIs from cells in the regions highlighted in the left panels were averaged from four  
751 experiments and plotted as a bar graph. Bar colors match the corresponding histograms. Error bars depict  
752 SEM. Ordinary one-way ANOVA was used for statistical analysis. In all bar graphs, values for individual  
753 data points are represented by closed shapes. **(B)** Left: CCRF-CEM-IKAROS-3 $\times$ FLAG cells were treated  
754 with Doxy for the indicated times. Example NOTCH3 flow cytometry histograms are shown. Right:  
755 NOTCH3 MFIs from four independent experiments were averaged and plotted as in (A). Error bars depict  
756 SEM. Ordinary one-way ANOVA was used for statistical analysis. **(C)** CCRF-CEM cells transduced with  
757 empty vector (V), wild type GFI1-3 $\times$ FLAG (GFI1), FLAG-tagged GFI1 lacking the N-terminal SNAG  
758 domain ( $\Delta$ SNAG) or FLAG-tagged GFI1 with a SNAG domain point mutant no longer able to interact with  
759 LSD1 (P2A). Cells were treated with vehicle (blue) or Doxy (red) for 48 hr. Left: representative flow  
760 cytometry histograms for NOTCH3 cell surface expression. Right: average MFIs from four independent  
761 experiments. Error bars depict SEM. Two-way ANOVA was used for statistical analysis. **(D)** Flow  
762 cytometry of CCRF-CEM-GFI1-3 $\times$ FLAG cells pre-treated with DMSO vehicle or LSD1 inhibitor (1  $\mu$ M  
763 SP-2509, MedKoo Biosciences) for 20 hr and subsequently treated with Doxy for 24 or 48 hr. DMSO or

764 SP-2509 was present continuously. Left: representative NOTCH3 flow cytometry. Right: MFIs within the  
765 NOTCH3-positive gates were averaged from four independent experiments and plotted as a bar graph. Error  
766 bars depict SEM. An unpaired T-test was used for statistical analysis.

767

768 **Figure 7. (A)** Flow cytometry for NOTCH3 cell surface expression in SUP-T1 cells transduced with vector  
769 or GFI1-3×FLAG inducible vectors and treated without or with doxycycline (Doxy), and SP-2509 for 48  
770 hr. Left: representative NOTCH3 flow cytometry. Right: NOTCH3 MFIs were averaged from four  
771 independent experiments and plotted as a bar graph. Error bars depict SEM. An unpaired T-test was used  
772 for statistical analysis. In each bar graph, values for each independent test are represented by closed shapes.

773 **(B)** SP-2509 abolishes the SNAG—LSD1 interaction. Biotinylated SNAG peptide demethylated at K8 was  
774 added to CCRF-CEM cell extracts with or without SP-2509 and incubated for 1 hr prior to addition of  
775 streptavidin-Sepharose beads to collect biotinylated peptide and bound LSD1. LSD1 in the bound and  
776 unbound fractions were visualized by western blot using anti-LSD1 antibody. **(C)** Flow cytometry of  
777 CCRF-CEM-GFI1-3×FLAG cells pretreated with DMSO or 2 μM lenalidomide (LEN) for 16 hr before  
778 treatment with Doxy for 48 hr. DMSO or Lenalidomide was present continuously. Left: example NOTCH3  
779 flow cytometry. Right: MFIs within the NOTCH3-positive regions shown at left were averaged from four  
780 independent experiments and plotted as a bar graph. Bar color corresponds to histogram shading on the left.  
781 Error bars depict SEM. Error bars depict SEM. Two-way ANOVA was used for statistical analysis. **(D)**

782 Flow cytometry of CCRF-CEM-GFI1-3×FLAG cells electroporated with control RNP or IKAROS RNPs  
783 as in Figure 5A. Cells were treated with Doxy for 0 or 48 hr. Left: example NOTCH3 flow cytometry.  
784 Right: MFIs within the NOTCH3-positive regions shown on the left were averaged from four independent  
785 experiments and plotted as a bar graph. Error bars depict SEM. Two-way ANOVA was used for statistical  
786 analysis.

787

788 **Figure 8. A proposed model of GFI1 mediated-noncanonical transcriptional activation.** In the well-  
789 known canonical transcriptional regulation mechanism, GFI1 acts as a transcriptional repressor by  
790 recruiting LSD1/CoREST-containing complexes via its SNAG domain. In non-canonical transcriptional  
791 activation, GFI1 activates NOTCH3 and other hallmark T cell developmental genes with IKAROS. DNA  
792 binding by both proteins is required, as is an intact SNAG domain not bound by LSD1. An LSD1 inhibitor,  
793 which blocks SNAG—LSD1 binding enables transactivation of *NOTCH3* and similarly regulated genes via  
794 the GFI1—IKAROS partnership.

795

796 **Supplementary Figure S1.** ChIP-Seq quality control data and motif analysis. (A) Correlation of GFI1 and  
797 IKAROS ChIP-Seq (and corresponding input) signaling. Spearman correlation R-values are displayed as a  
798 heatmap. (B) Principal component analysis (PCA) plot and cluster analysis of all ChIP-Seq samples. (C)  
799 Motif analysis (HOMER) showing enriched motifs within GFI1 and IKAROS ChIP-Seq peaks. The top 5  
800 nonredundant motifs ranked by statistical significance are shown.

801

802 **Supplementary Figure S2.** GFI1 and IKAROS binding and expression data for genes encoding other  
803 Notch family members. IGV tracks displaying GFI1 and IKAROS ChIP-Seq and RNA-Seq read  
804 distribution similar to Figure 5C, except for *NOTCH1*, *NOTCH2*, and *NOTCH4*.

805

806 **Supplementary Figure S3.** Lenalidomide treatment or CRISPR RNP transfection rapidly depletes  
807 IKAROS protein while maintaining inducible GFI1 expression. (A) IKAROS Western blot of  
808 Lenalidomide (LEN)-treated CCRF-CEM GFI1-3×FLAG cells. Lysates were prepared from untreated (0  
809 hr) cells, and over a 64 hr time course.  $\beta$ -actin is shown as a loading control. (B) Lysates from the same  
810 cells as in (A) were immunoblotted using GFI1 antibodies. (C) IKAROS Western blot using lysates from  
811 CCRF-CEM GFI1-3×FLAG cells electroporated with control or IKAROS RNP. Cells were prepared

812 similarly as in Figure 5A. **(D)** Lysates from the same cells as in (C) were immunoblotted using GF11  
813 antibodies.

814

#### 815 **Tables and their legends**

816 **Supplemental Table S1.** BioID mass spectrometry results (average intensity of WT<=VEC and three  
817 triplicates T-test (BirA\* vs WT) *P*-value  $\geq 0.05$ , the data were deleted), 502 proteins.

818

819 **Supplemental Table S2.** Gene Ontology (GO) enrichment analysis of GF11 and IKAROS ChIP-Seq peaks.

820

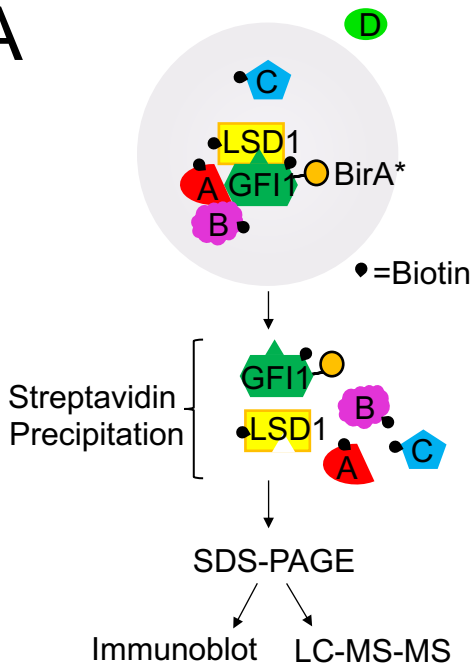
821 **Supplemental Table S3.** RNA-Seq differential gene expression.

822

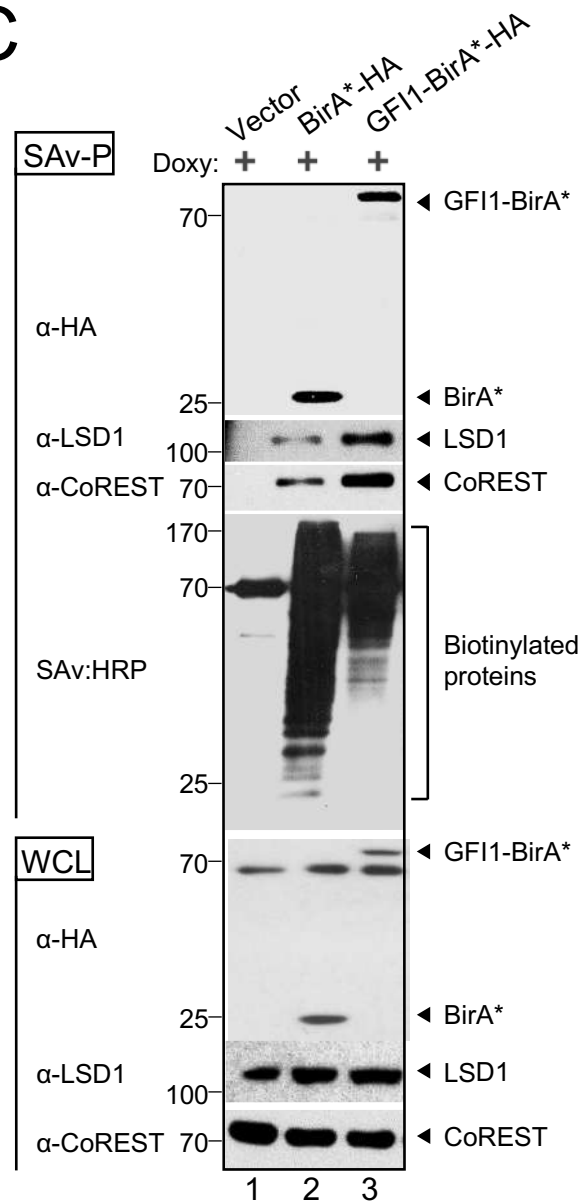
823 **Supplemental Table S4.** List of genes within cluster 4 of Figure 5B and distance from TSS to the nearest  
824 GF11 or IKAROS peak center.

# Sun et al. Figure 1

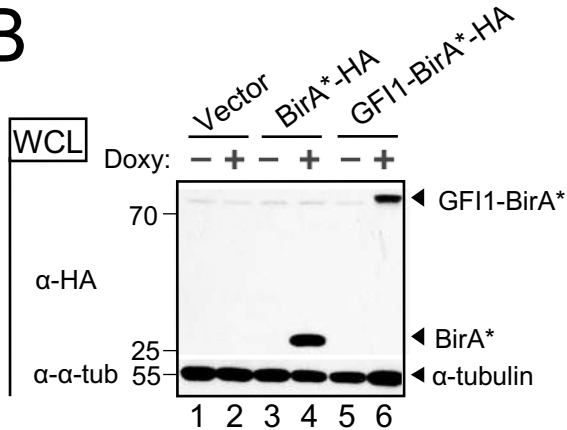
## A



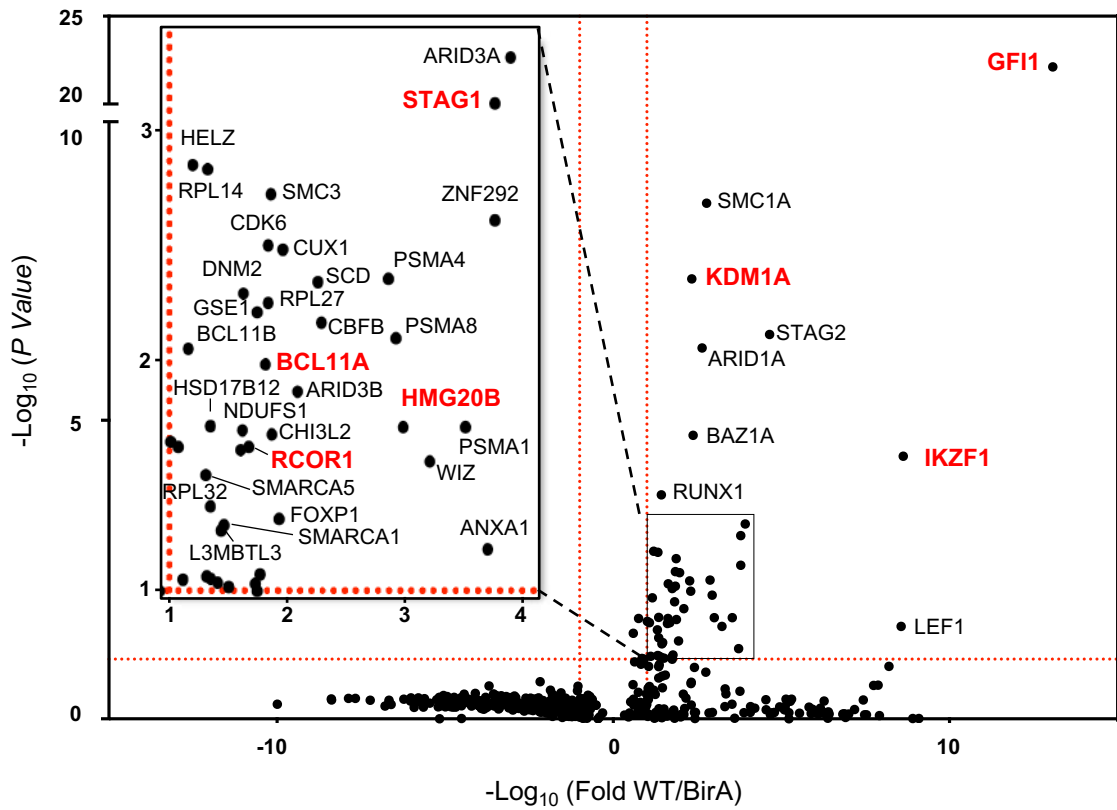
## C



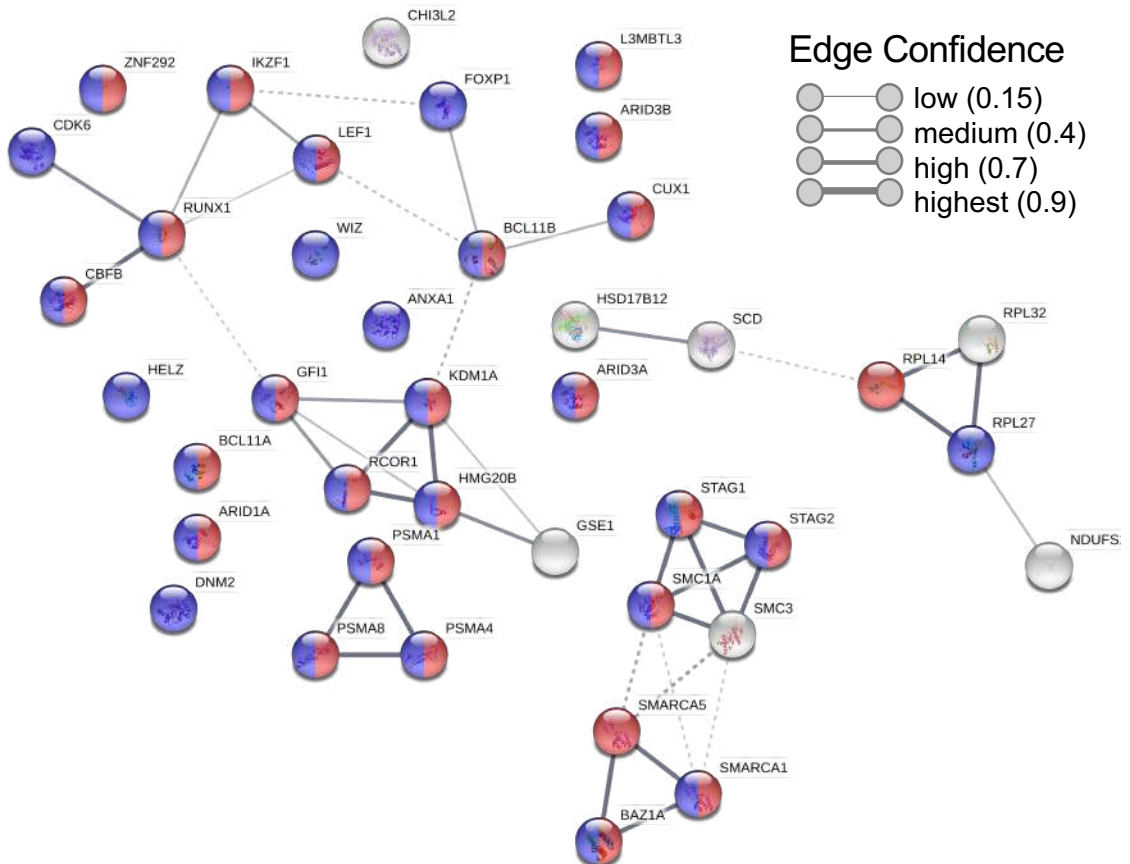
## B

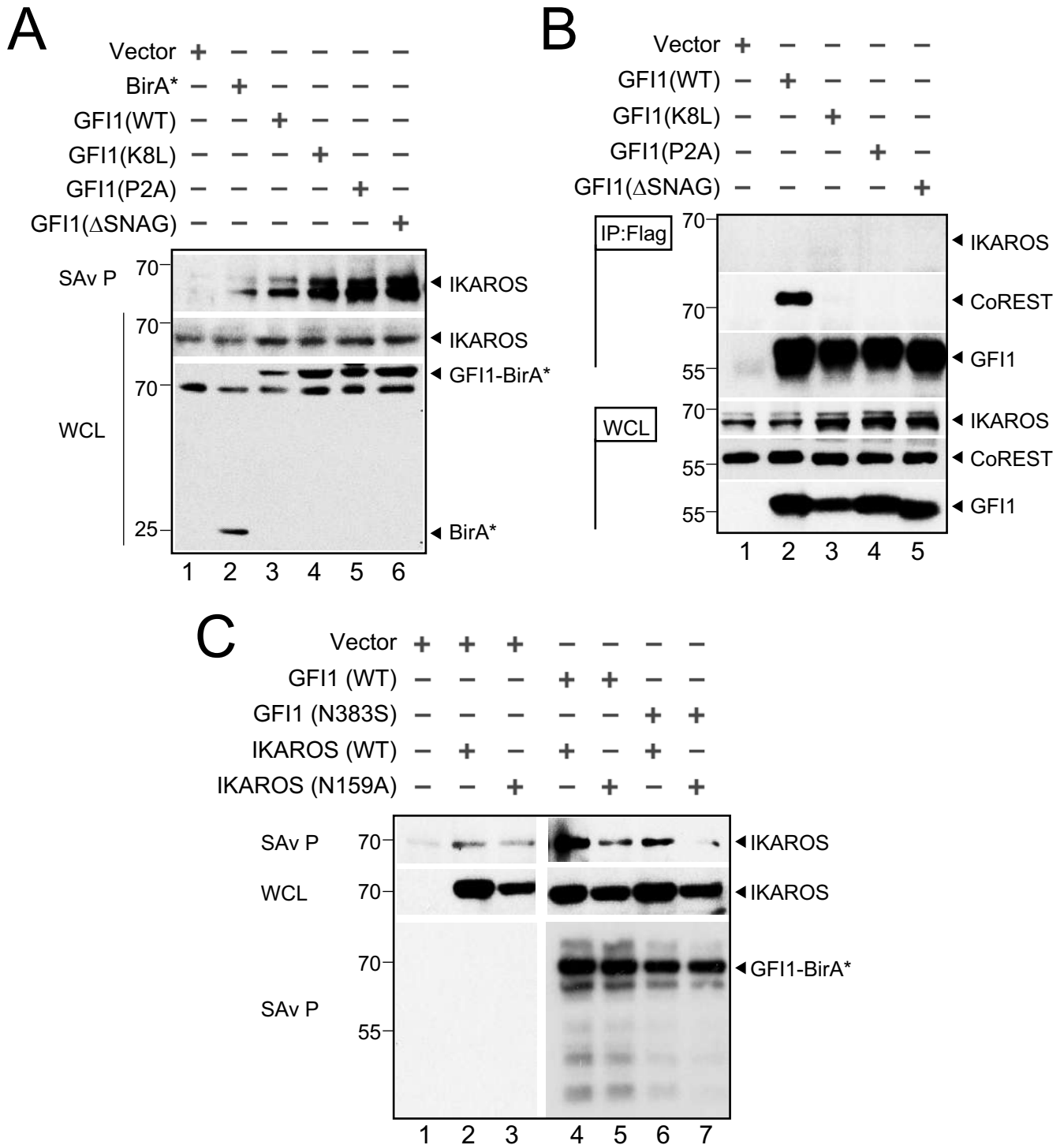


A

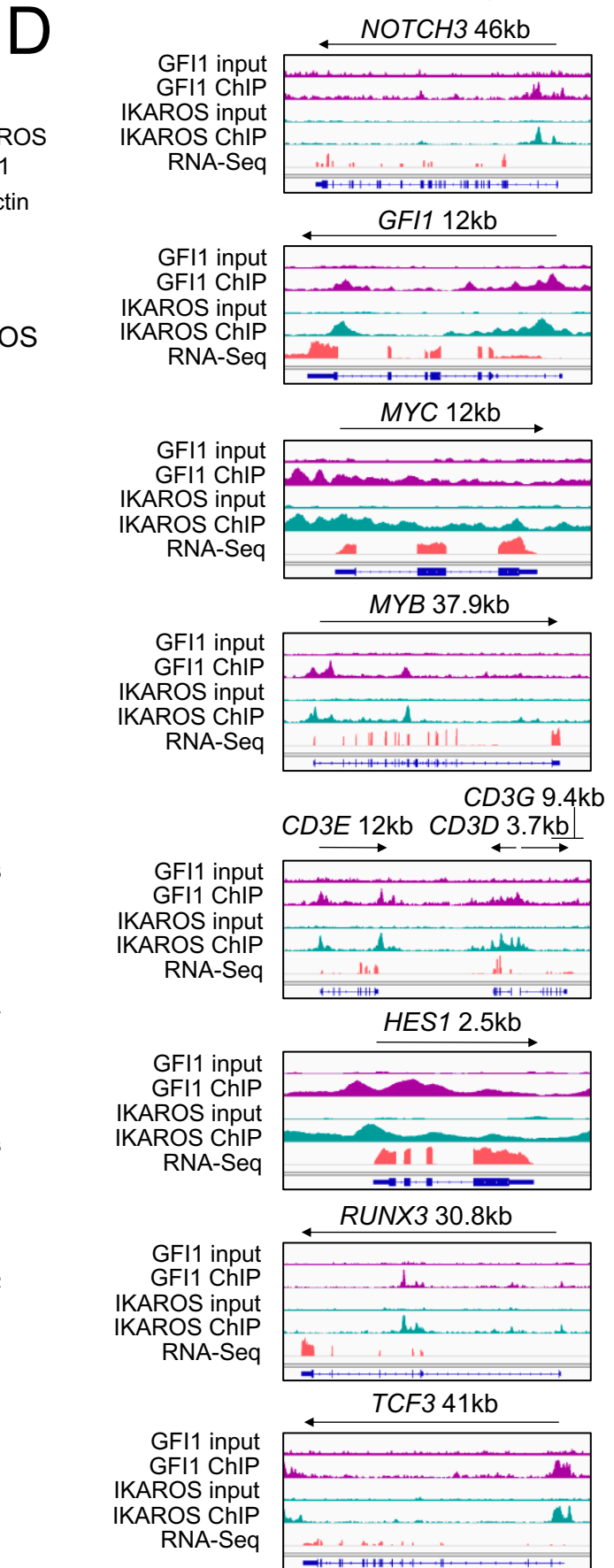
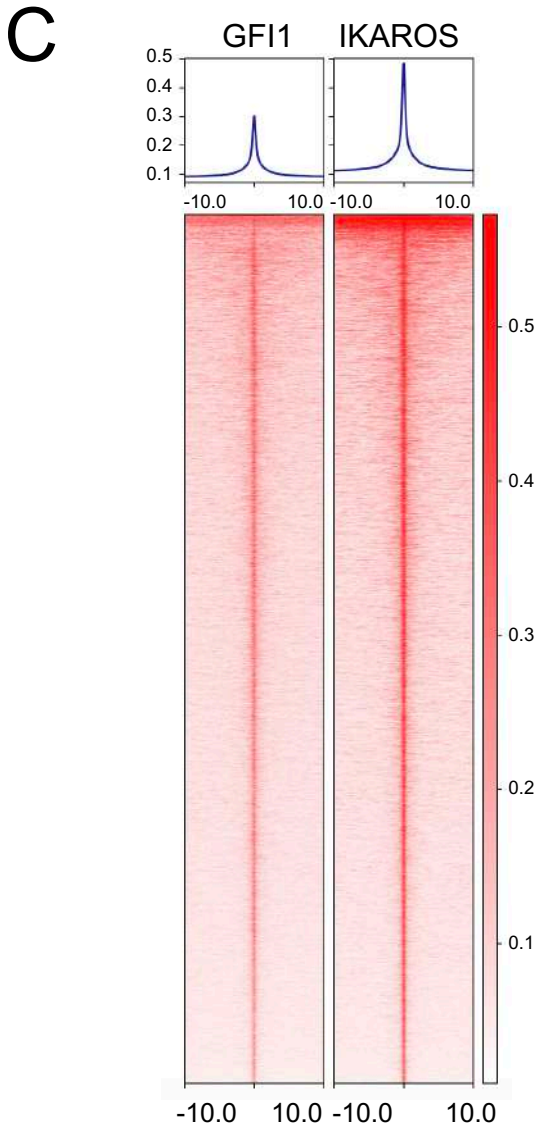
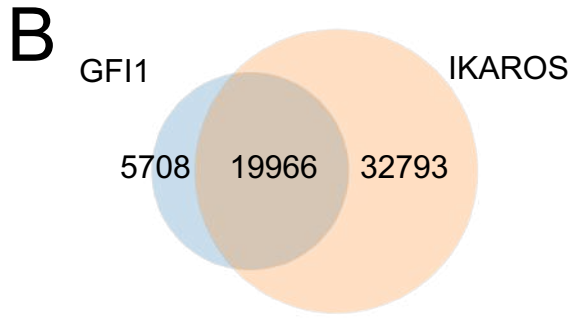
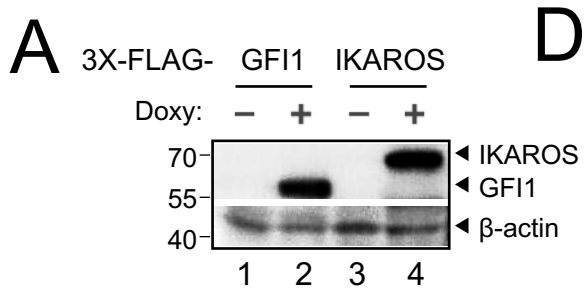


B

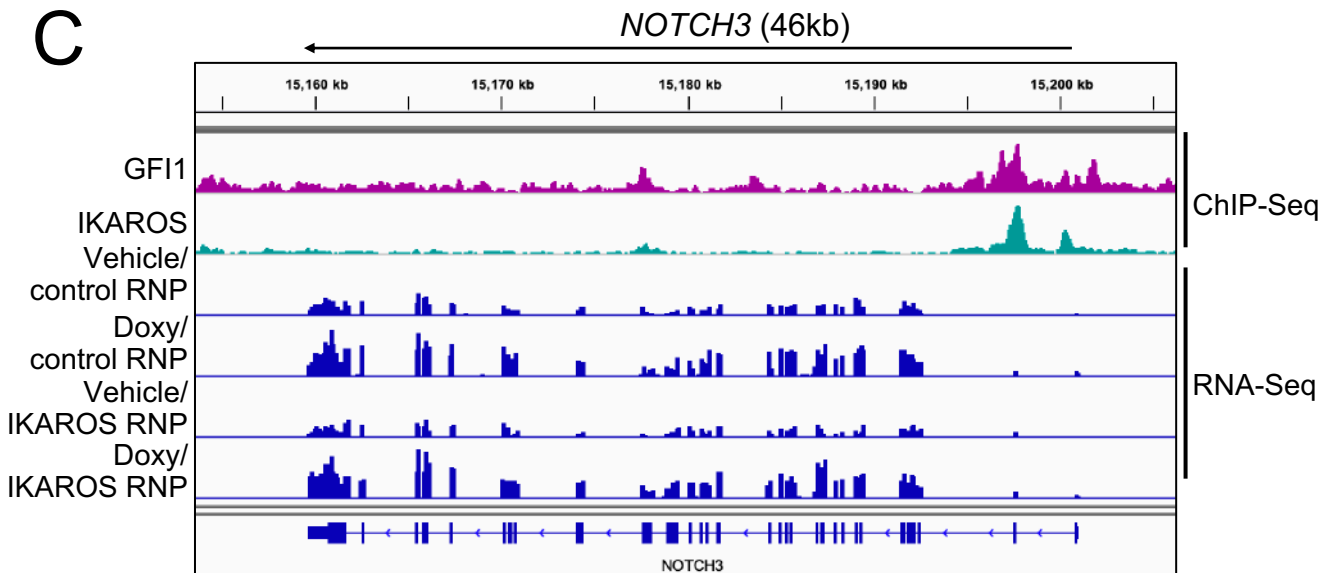
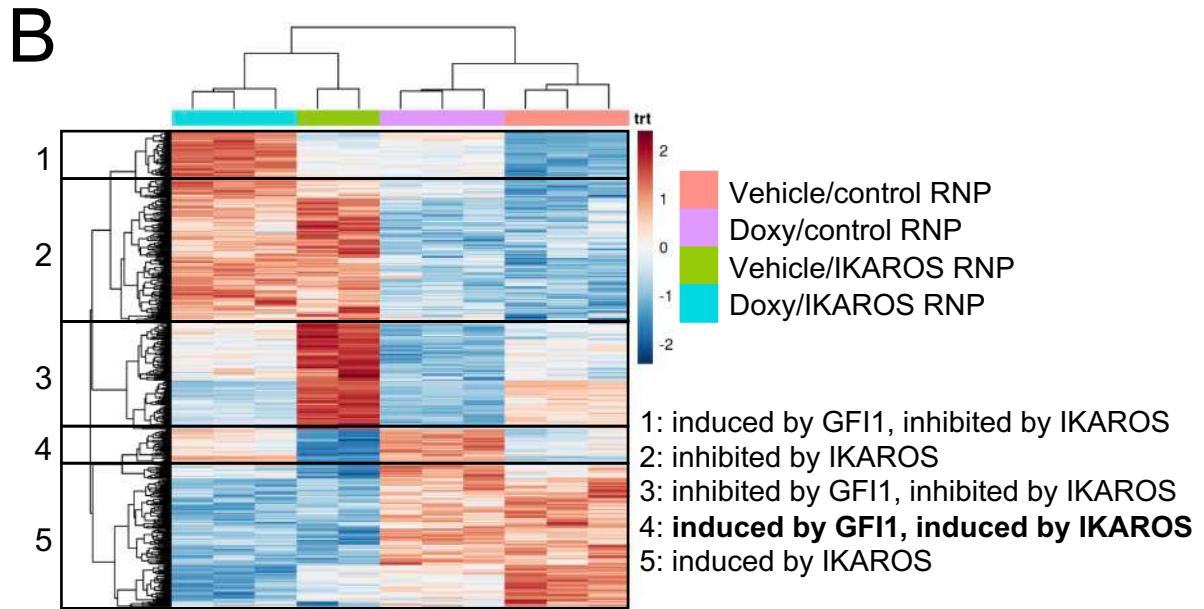
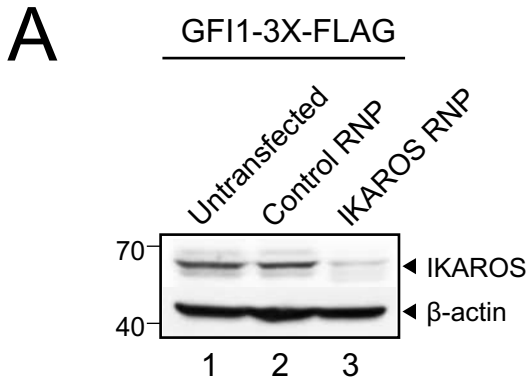


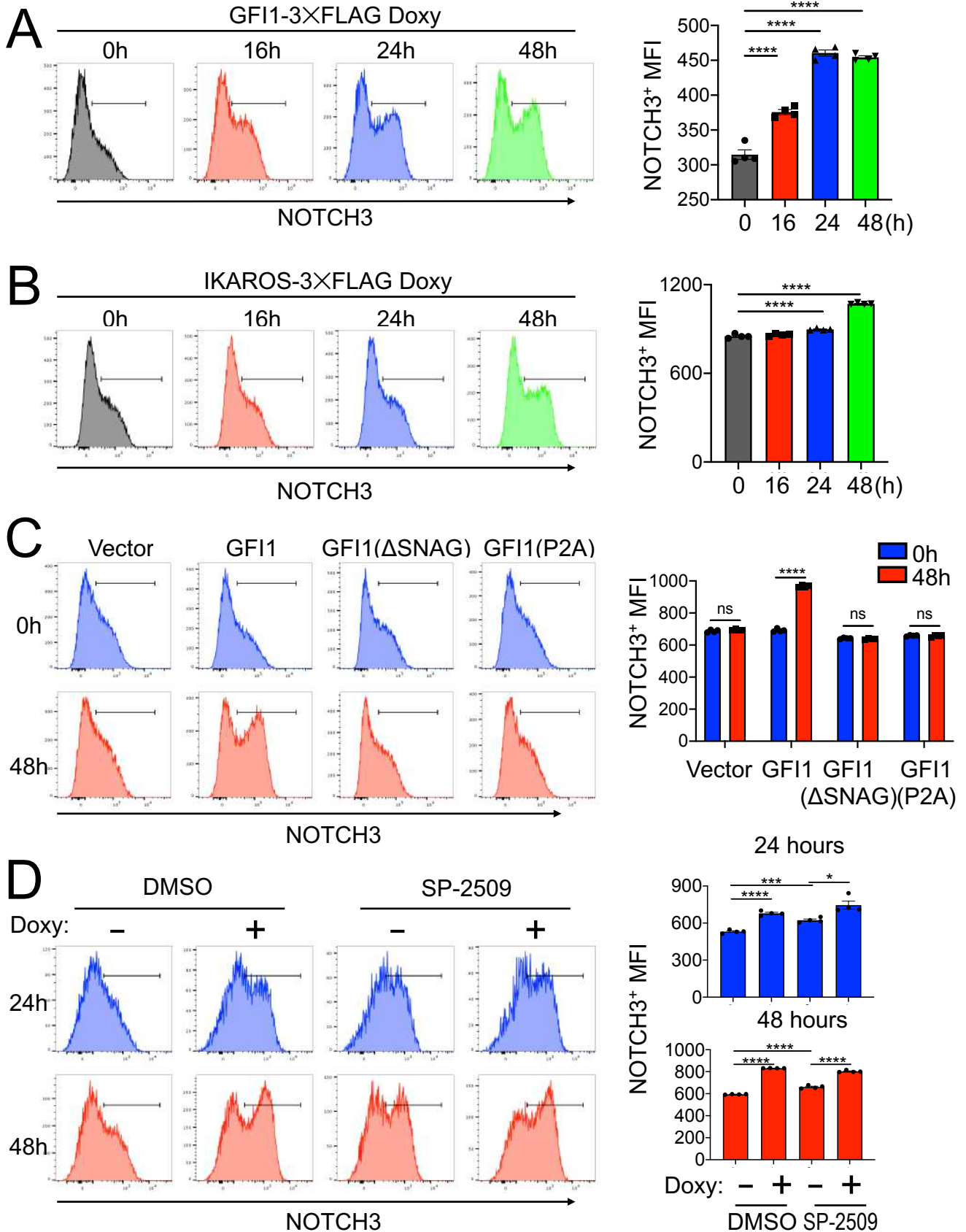


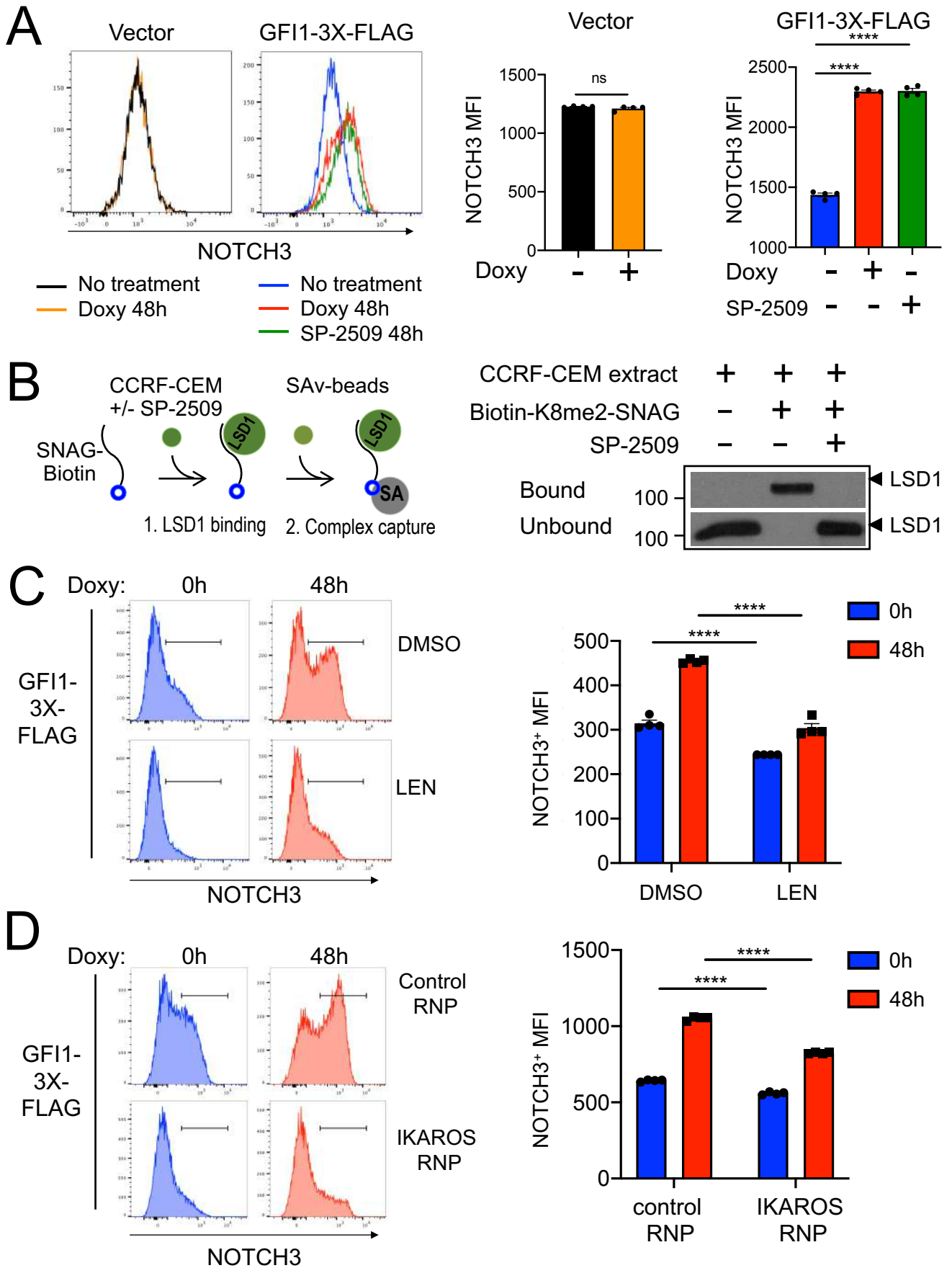
# Sun et al. Figure 4

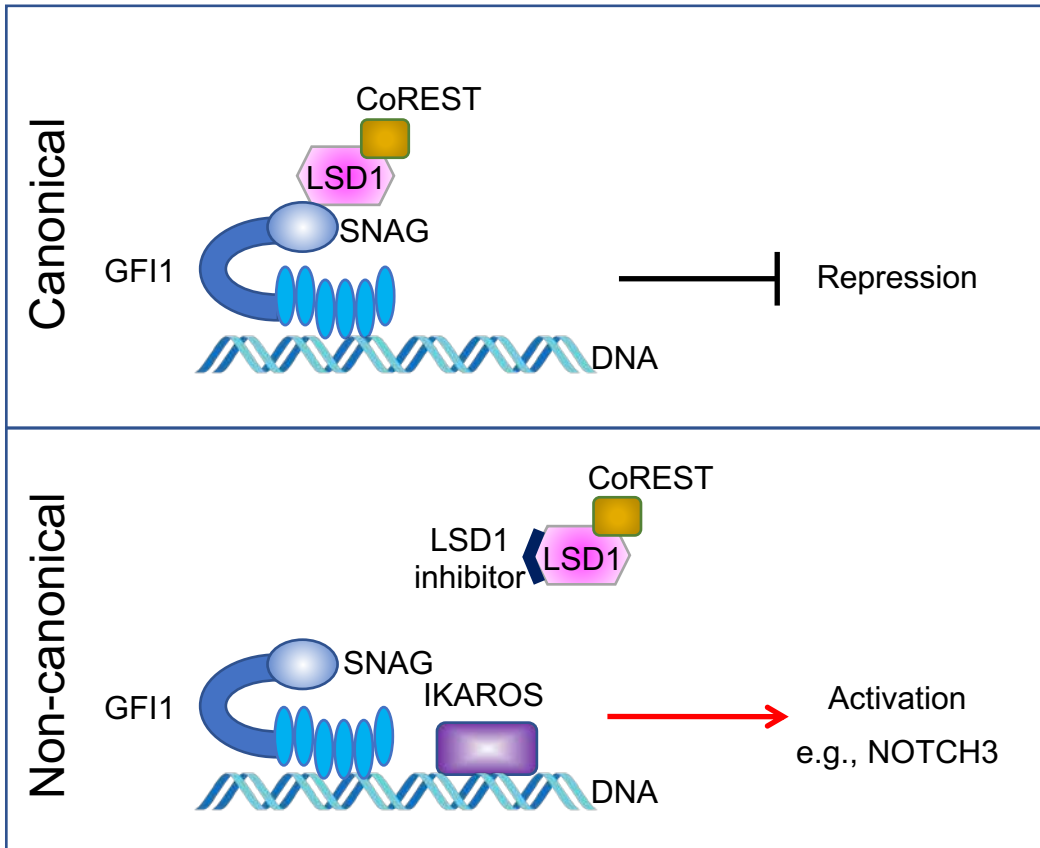




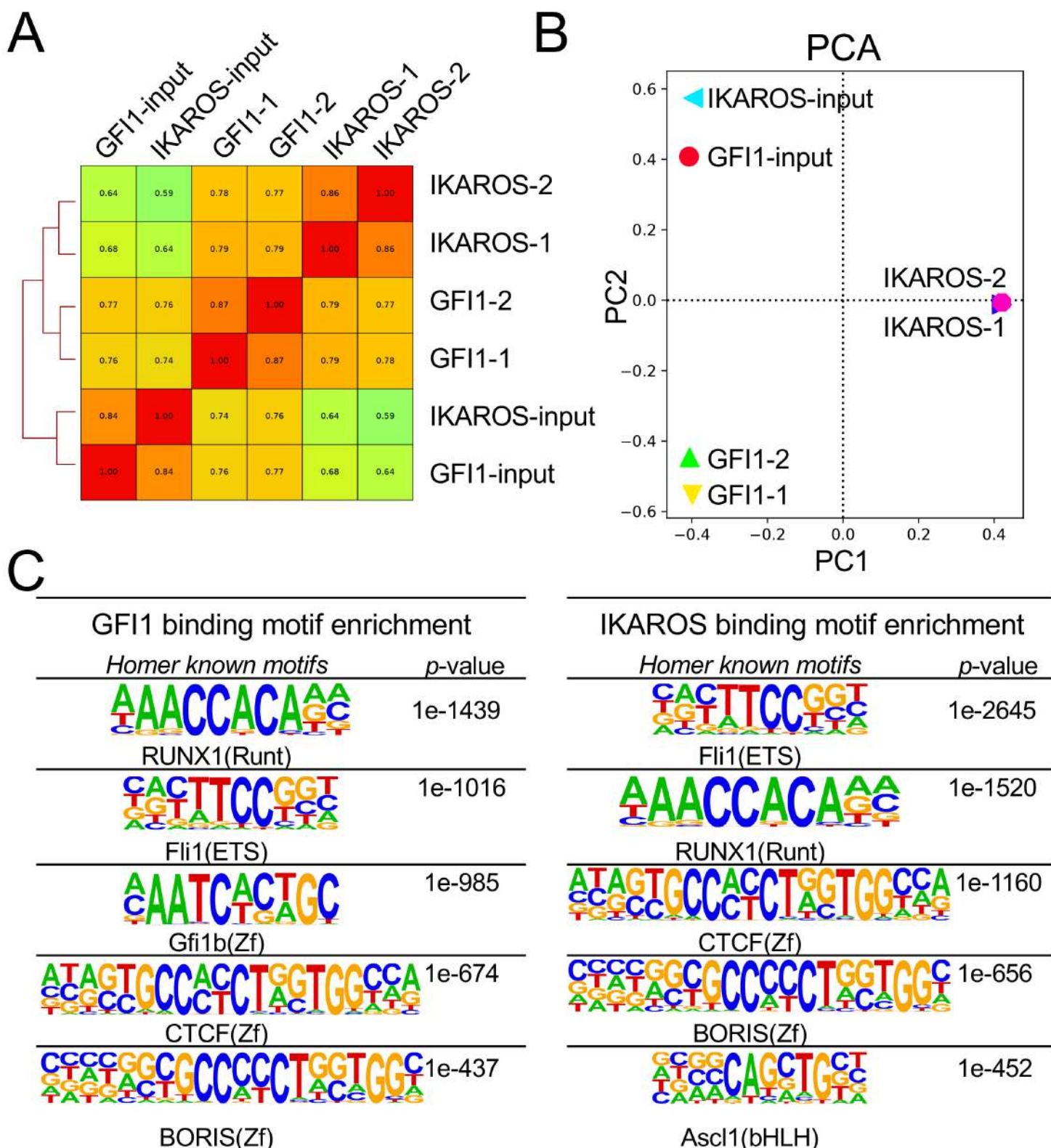








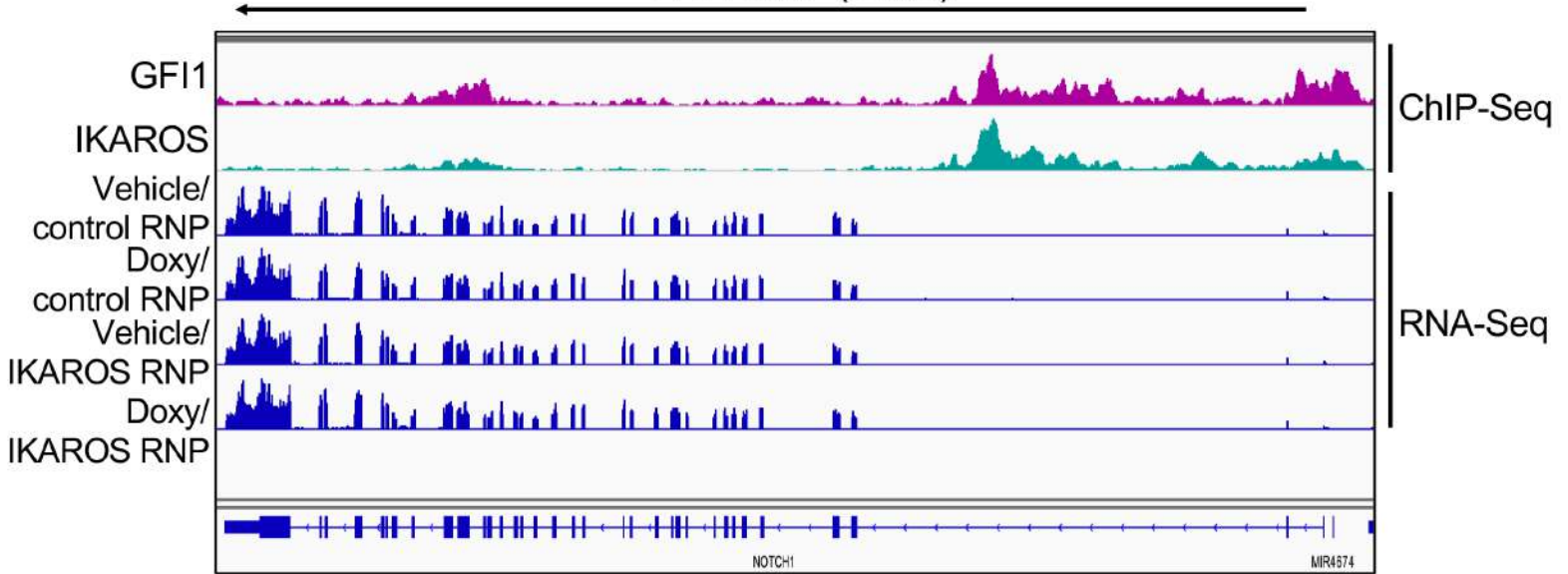
# Sun et al. Supplemental Figure 1



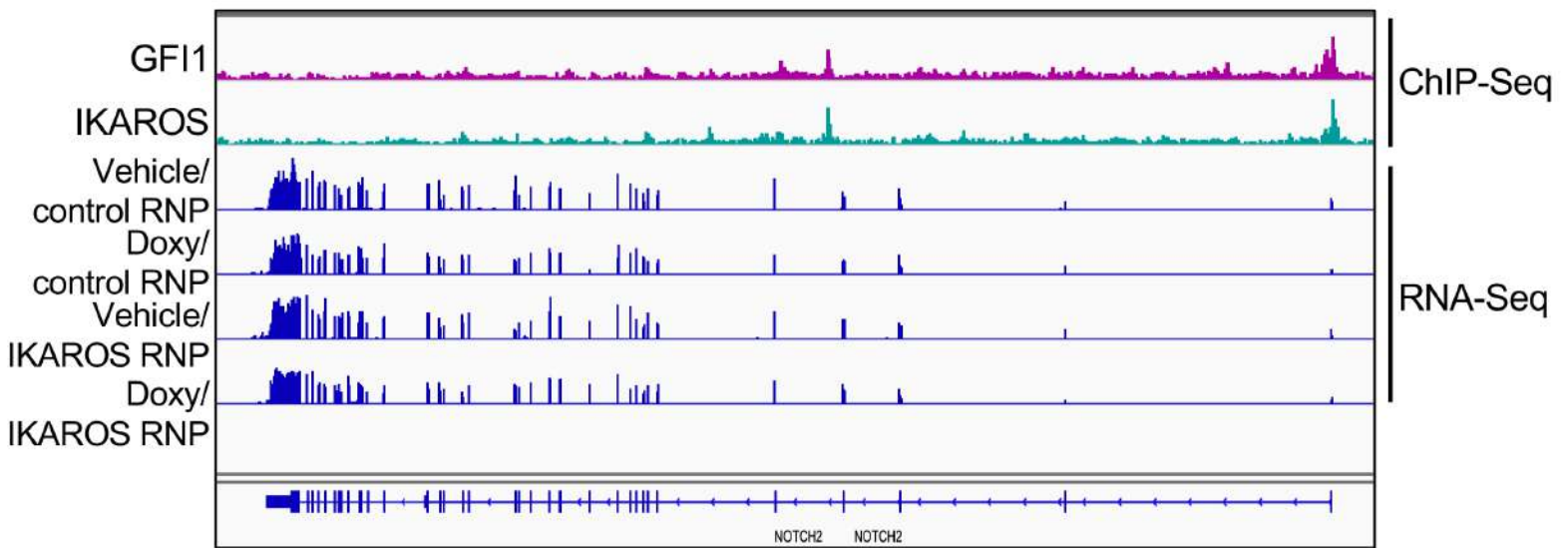


# Sun et al. Supplemental Figure 2

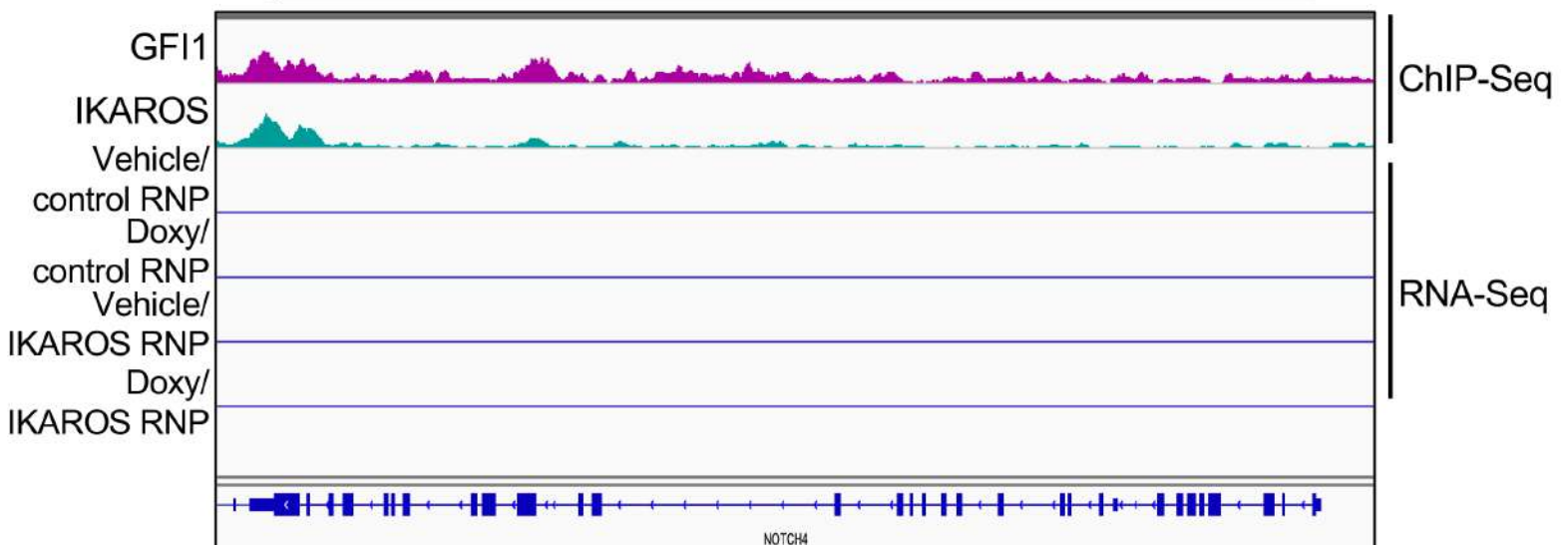
## *NOTCH1* (51kb)



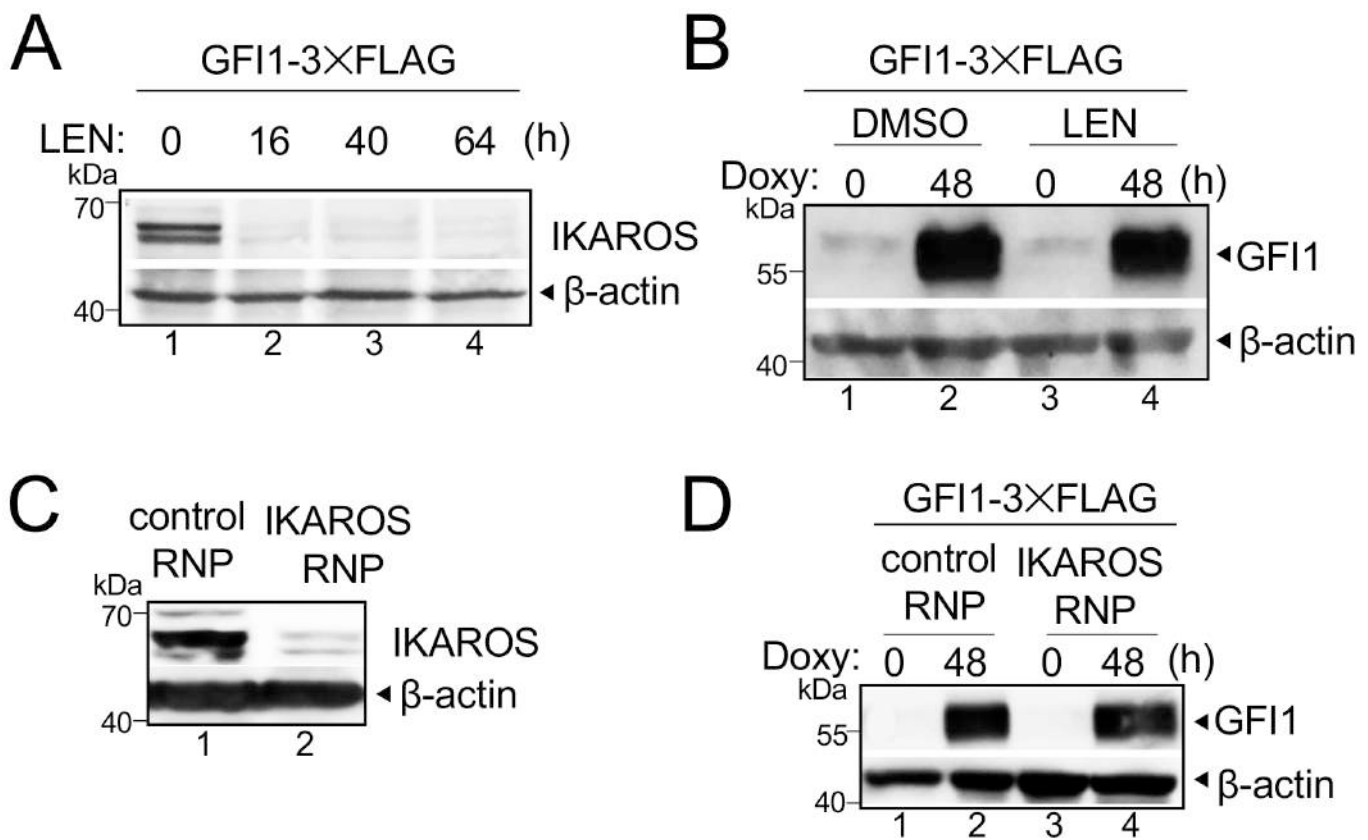
## *NOTCH2* (158kb)



## *NOTCH4* (33kb)



# Sun et al. Supplemental Figure 3



Sun et al. Supplemental Table S2: Gene Ontology (GO) enrichment analysis

Gene Ontology (GO) enrichment analysis with GF		
Rank	Term Name	P-Value
1	regulation of gene expression, epigenetic	7.0764E-85
2	regulation of hematopoietic progenitor cell differentiation	3.4017E-68
3	regulation of hematopoietic stem cell differentiation	4.4564E-62
4	negative regulation of gene expression, epigenetic	4.3610E-52
	somatic diversification of immune receptors via germline	
5	recombination within a single locus	1.8269E-40
6	V(D)J recombination	2.1433E-39
7	somatic diversification of immune receptors	5.8618E-39
8	regulation of megakaryocyte differentiation	3.3875E-38
9	DNA replication-dependent nucleosome assembly	7.4252E-38
10	positive regulation of viral life cycle	2.0917E-33
11	positive regulation of gene expression, epigenetic	3.2093E-32
12	chromatin silencing	6.7381E-31
13	positive regulation of myeloid leukocyte differentiation	6.9143E-31
14	beta-catenin-TCF complex assembly	1.9700E-28
15	chromatin silencing at rDNA	3.6319E-28
	intrinsic apoptotic signaling pathway in response to DNA	
16	damage	4.8943E-27
	positive regulation of protein insertion into mitochondrial	
17	membrane involved in apoptotic signaling pathway	7.0662E-22

Gene Ontology (GO) enrichment analysis with IKA		
Rank	Term Name	P-Value
1	regulation of hematopoietic progenitor cell differentiation	1.1371E-61
2	regulation of hematopoietic stem cell differentiation	1.8733E-52
3	B cell receptor signaling pathway	4.4539E-40
	positive regulation of mitochondrial outer membrane	
4	permeabilization involved in apoptotic signaling pathway	7.3392E-34
5	somatic diversification of immune receptors	1.1375E-32
6	regulation of T cell receptor signaling pathway	3.9032E-26

\*The GO analysis was performed using GREAT tool (v 4.0.4) following its default settings.



of GFI1 and IKAROS ChIP-SEQ peaks\*

GFI1 binding peaks		
Fold Enrichment	Observed Gene Hits	Total Genes
2.1208	209	248
2.7850	92	113
2.8136	86	103
2.5319	93	114
2.9966	31	32
3.6440	14	14
2.7361	36	38
2.2967	65	76
7.2147	29	32
2.0164	78	98
2.4171	70	80
2.4221	78	97
2.0172	45	50
2.1595	39	43
4.0207	35	36
2.1653	57	69
2.3287	27	29

IKAROS binding peaks		
Fold Enrichment	Observed Gene Hits	Total Genes
2.1139	107	113
2.0869	97	103
2.0451	35	35
2.079	37	37
2.0353	38	38
2.0342	36	36

**Sun et al. Supplemental Table S4: List of genes within cluster 4 of Figure 5B and distance from TSS to th**

Gene name

Plectin

SH3 Domain And Tetratricopeptide Repeats 1

Sphingomyelin Phosphodiesterase 3

LIM Zinc Finger Domain Containing 2

BAH Domain And Coiled-Coil Containing 1

Inositol-3-Phosphate Synthase 1

Proline-Rich Protein 36

Tescalcin

ADAMTS-Like Protein 2

Tumor Protein P73

AT-Rich Interactive Domain-Containing Protein 3A

Protein Tyrosine Phosphatase Non-Receptor Type 6

RAS Guanyl Releasing Protein 2

Myosin VIIB

Proteasome 20S Subunit Beta 8

Transporter 1, ATP Binding Cassette Subfamily B Member

RAS P21 Protein Activator 3

MX Dynamin Like GTPase 1

Adhesion G Protein-Coupled Receptor B2

CAMP Responsive Element Binding Protein 3 Like 3

Meteorin, Glial Cell Differentiation Regulator

Glutamate Receptor, Ionotropic, N-Methyl D-Aspartate-Associated Protein 1 (Glutamate Binding

Y-Box Binding Protein 2

Semaphorin 7A

Recombination Activating 1

IL2 Inducible T Cell Kinase

Palladin, Cytoskeletal Associated Protein

Mindbomb E3 Ubiquitin Protein Ligase 1

Notch Receptor 3

Dematin Actin Binding Protein

Calcium And Integrin Binding Family Member 2

Collagen Type XVIII Alpha 1 Chain

Cadherin EGF LAG Seven-Pass G-Type Receptor 2

Hydroxyacylglutathione Hydrolase-Like Protein

Glutamate-Ammonia Ligase

Adenine Nucleotide Translocase Lysine N-Methyltransferase

Insulin Receptor Substrate 1

Protein Kinase CAMP-Activated Catalytic Subunit Beta

**ie nearest GFI1 or IKAROS peak center.**

Gene symbol	TSS (Hg38)	distance to nearest GFI1 peak center (kb)
PLEC	chr8:143,976,745	4.1
SH3TC1	chr4:8,199,244	0
SMPD3	chr16:68,448,506	4.1
LIMS2	chr8:143,976,745	1.8
BAHCC1	chr17:81,399,721	0
ISYNA1	chr19:18,438,301	15.6
PRR36	chr19:7,874,441	69.8
TESC	chr12:117,099,446	0
ADAMTSL2	chr9:9,133,532,164	2.6
TP73	chr1:3,652,565	31.2
ARID3A	chr19:926,037	52.4
PTPN6	chr12:6,946,577	1.7
RASGRP2	chr15:3,856,486	0.5
MYO7B	chr2:127,535,802	8.7
PSMB8	chr6:32,844,935	0.2
TAP1	chr6:32,853,971	0.2
RASA3	chr13:114,132,623	1.2
MX1	chr2:41,420,558	58.7
ADGRB2	chr1:31,764,063	40
CREB3L3	chr19:4,153,601	28.9
METRN	chr16:715,173	5.9
GRINA	chr8:143,990,058	11.5
YBX2	chr17:7,294,559	13.8
SEMA7A	chr15:74,433,959	4.8
RAG1	chr11:36,568,013	0.1
ITK	chr5:157,180,896	0
PALLD	chr4:168,497,066	15.8
MIB1	chr18:21,741,329	1.2
NOTCH3	chr19:15,200,981	0.8
DMTN	chr8:22,048,955	0.2
CIB2	chr15:78,131,535	0.1
COL18A1	chr21:45,405,137	73.3
CELSR2	chr1:109,250,019	35.1
HAGHL	chr16:726,936	5.8
GLUL	chr1:182,392,206	0.4
ANTKMT	chr16:721,142	0
IRS1	chr2:226,798,790	3.9
PRKACB	chr1:84,077,975	0.3

distance to nearest IKAROS peak center (kb)	GF11 and IKAROS peaks <10 kb	GF11 and IKAROS peaks
4.2	Yes	No
0.5	Yes	Yes
4.2	Yes	No
1.7	Yes	No
0	Yes	Yes
8.3	No	No
5.8	No	No
0.1	Yes	Yes
1.4	Yes	No
24.7	No	No
0.3	No	No
2.2	Yes	No
0.2	Yes	Yes
9.9	Yes	No
0.2	Yes	Yes
0.2	Yes	Yes
0.8	Yes	No
0.1	No	No
6.9	No	No
13.1	No	No
0.1	Yes	No
3.7	No	No
0.4	No	No
0.2	Yes	No
0.1	Yes	Yes
0	Yes	Yes
12	No	No
0.3	Yes	No
0.6	Yes	No
0.1	Yes	Yes
0.1	Yes	Yes
8.6	No	No
33.2	No	No
0.2	Yes	No
0.2	Yes	Yes
0	Yes	Yes
0.9	Yes	No
0.2	Yes	Yes

<500 bp